Lithos 182–183 (2013) 134–149

Contents lists available at ScienceDirect

Lithos

journal homepage: www.elsevier.com/locate/lithos

The campsite dykes: A window into the early post-solidification history of the Skaergaard Intrusion, East Greenland ☆

Marian B. Holness [a,*], Chris Richardson [b], Jens C.Ø. Andersen [c]

[a] Department of Earth Sciences, University of Cambridge, Downing Street, Cambridge CB2 3EQ, UK
[b] BP Institute, Bullard Laboratories, Madingley Road, Cambridge CB3 0EZ, UK
[c] Camborne School of Mines, College of Engineering, Mathematics and Physical Sciences, University of Exeter, Penryn, Cornwall TR10 9EZ, UK

ARTICLE INFO

Article history:
Received 3 July 2013
Accepted 5 October 2013
Available online 14 October 2013

Keywords:
Microstructure
Dihedral angle
Dyke
Cumulate
Layered intrusion

ABSTRACT

The Skaergaard Intrusion of East Greenland is cut by several generations of dykes, the earliest of which is thought to have intruded shortly after solidification of the Skaergaard. Two ~6 m wide doleritic dykes from the earliest generation are exposed in the campsite area near Homestead Bay of the Skaergaard Peninsula. One of the dykes (the Campsite Dyke) locally contains abundant xenoliths of troctolitic cumulate. The other (the Plagioclase-phyric Dyke) contains abundant large plagioclase phenocrysts. Cross-cutting relationships between the two dykes are not exposed. The median clinopyroxene–plagioclase–plagioclase dihedral angle, Θ_{cpp}, in the Campsite Dyke is 88–89.5°, whereas that of the Plagioclase-phyric Dyke is 79°. Using an empirical relationship between Θ_{cpp} and the duration of crystallisation derived from dolerite sills, the observed Θ_{cpp} suggests that the Campsite Dyke is the older of the two, intruding the Skaergaard when it had cooled to 920–970 °C. The Plagioclase-phyric Dyke intruded later, once the Skaergaard had cooled below 670 °C. The troctolitic xenoliths divide into two separate groups. Type A xenoliths have microstructures similar to those of the Skaergaard Layered Series although mineral compositions are generally more primitive than those of the exposed cumulates — this type of xenolith is likely to have been derived from either deeper levels in the Skaergaard Intrusion or from a closely-related underlying magma chamber. One Type A xenolith has mineral compositions and Θ_{cpp} consistent with an origin in LZb of the Layered Series — this xenolith contains partially inverted pigeonite, suggesting that inversion of low-Ca pyroxene in the lower part of the Layered Series took place after the intrusion had completely solidified. Type B xenoliths are characterized by plagioclase containing large and abundant melt inclusions. Comparison with the microstructures of glassy crystalline nodules from Iceland points to a multi-stage cooling history for Type B xenoliths, consistent with step-wise entrainment of partially crystallised material from a deep chamber. Type B xenoliths are very unlikely to have been derived from deeper levels in the Skaergaard chamber.

1. Introduction

The Skaergaard Intrusion of East Greenland formed during the Tertiary opening of the North Atlantic Ocean. Since the seminal work of Wager and Deer (1939) it has become one of the most important natural laboratories for understanding the progressive fractionation of basaltic magma. A suite of cumulate xenoliths in a large dyke that cuts the intrusion has the potential to provide information about the geology underlying the exposed parts of the Skaergaard chamber (Jakobsen et al., 2010). The xenoliths and their enclosing dyke present not only an opportunity to discover more about the deeper parts of the Layered Series and the associated magmatic plumbing system but, if the timing of intrusion can be established, microstructures in the xenoliths can be used to create a snapshot of the thermal profile through the Skaergaard Intrusion at the moment of entrainment and dyke injection.

In this contribution we demonstrate how it is possible to constrain the timing of dyke intrusion relative to the age of the host Skaergaard Intrusion from the geometry of three-grain junctions in the dyke groundmass. A microstructural analysis of a selection of xenoliths is then used to identify those most likely to have been derived from lower levels of the Skaergaard Intrusion, enabling us to place preliminary qualitative constraints on the cooling history of the Skaergaard.

2. Geological setting of the dykes

The Tertiary Skaergaard Intrusion of East Greenland coast comprises approximately 280 km^3 of basaltic magma intruded at the shallow crustal unconformity between Precambrian gneisses and overlying Tertiary flood basalts into a fault-bounded magma chamber (Nielsen, 2004) formed at the extending continental margin (Fig. 1). The magma crystallised as a closed system, forming three sequences of layered cumulates: the volumetrically dominant Layered Series which

* Corresponding author. Tel.: +44 1223 333400.
E-mail address: marian@esc.cam.ac.uk (M.B. Holness).

0024-4937/$ – see front matter © 2013 The Authors. Published by Elsevier B.V. All rights reserved.
http://dx.doi.org/10.1016/j.lithos.2013.10.007

crystallised from the floor of the intrusion upwards; the Marginal Border Series which crystallised from the sides of the chamber; and the Upper Border Series which crystallised downwards from the roof (Wager and Deer, 1939). The Upper Border Series and the Layered Series meet at the Sandwich Horizon. Within each series, mineral composition varies systematically from primitive to more evolved, consistent with uninterrupted fractional crystallisation. Boundaries between mineral assemblages divide the Layered Series into the Lower Zone (LZ), Middle Zone (MZ) and Upper Zone (UZ), with equivalent subdivisions for the Marginal Border Series (Hoover, 1989) and Upper Border Series (Salmonsen and Tegner, 2013). The unexposed lower part of the intrusion is known as the Hidden Zone (HZ), and has been sampled by a 350 m drill core (the Cambridge 1966 drill core) that is thought to intersect the lower contact of the intrusion (Holness et al., 2007a; Maaløe, 1976).

The Skaergaard Intrusion is cut by two generations of steeply dipping Tertiary dykes that form part of the coastal dyke swarm of East Greenland (Brooks and Nielsen, 1978; Nielsen, 1978). The earlier of the two generations cutting the Skaergaard comprises predominantly north–south trending basaltic and doleritic dykes (Fig. 2) of the group designated THOL-2 by Nielsen (1978). The later generation is camptonitic with an approximately east–west trend (Fig. 2; Vincent, 1953) and has been designated ALK-2 by Nielsen (1978). The spatial relationships between these two generations are clearly exposed just

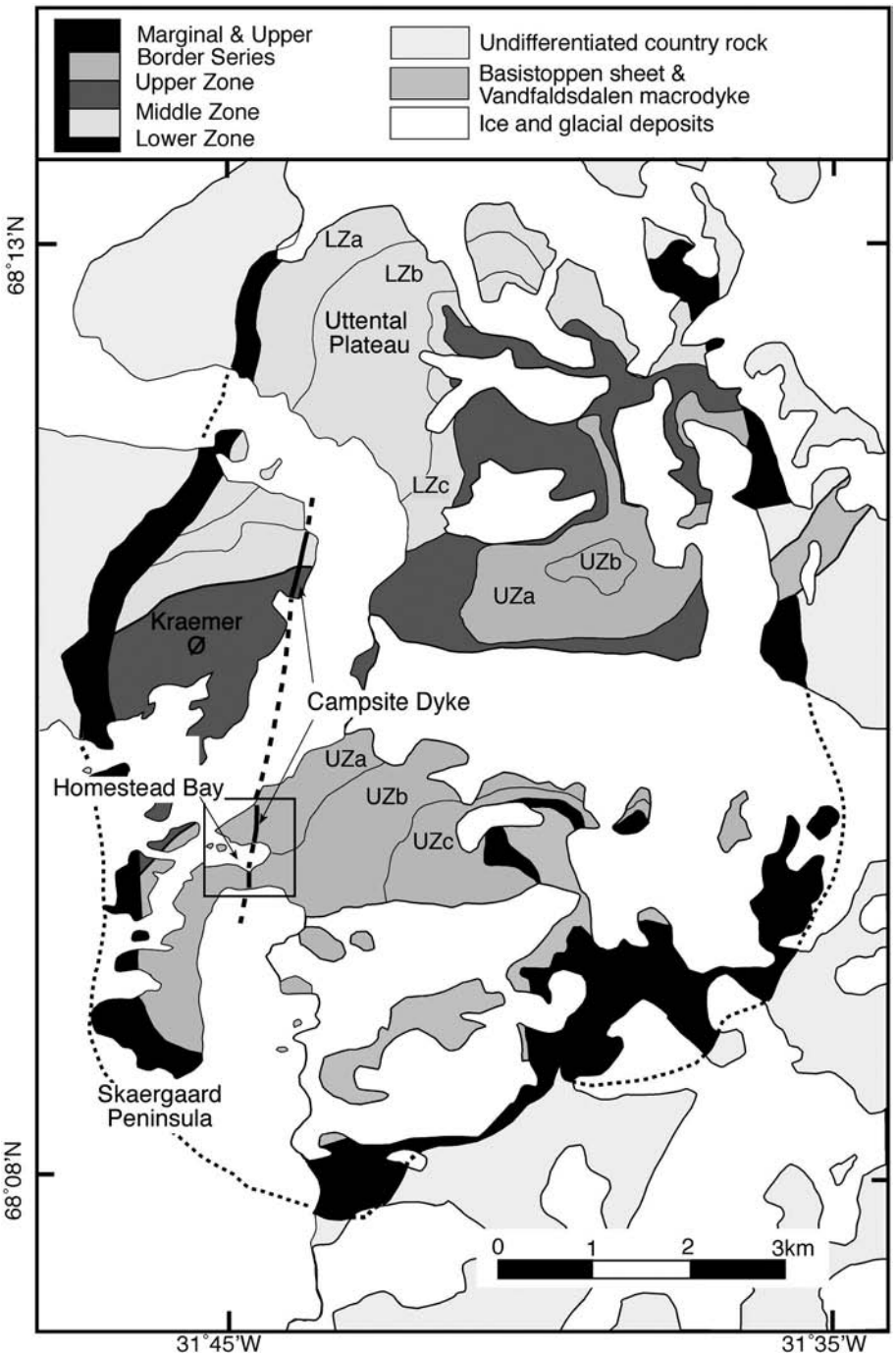

Fig. 1. Sketch map of the Skaergaard Intrusion. The square shows the area covered in Fig. 2. The Campsite Dyke is marked, including the suggested continuation on Kraemer Island. For clarity the Plagioclase-phyric Dyke is not marked.

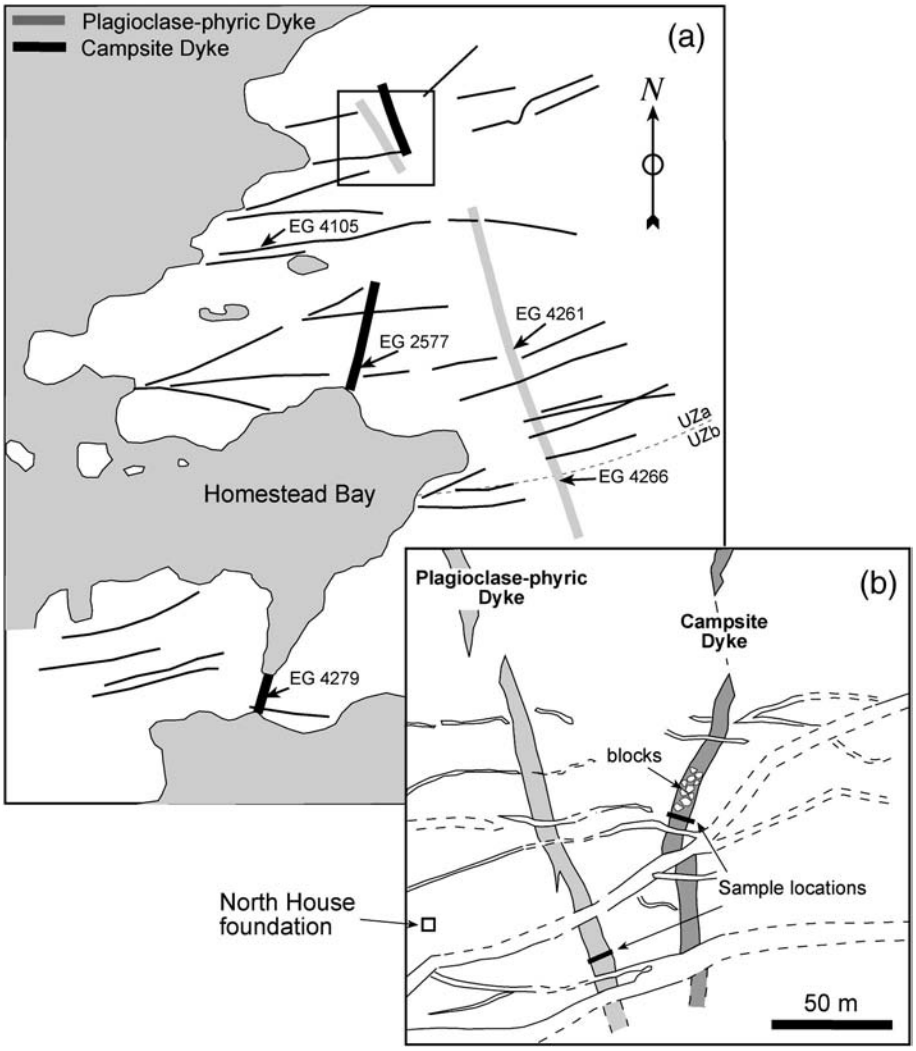

Fig. 2. (a) Map of dyke locations in the Campsite and Homestead Bay area, based on Vincent (1953), with a coastline taken from the modern map. Note the two generations of dykes, with the older one shown as heavy lines and the later, E/W trending population as thinner lines. The locations of samples collected by L.R. Wager (prefix EG) and examined as part of this study are shown. These are housed in the Oxford Museum of Natural History. The square box shows the location of the map in (b). (b) Detailed map of the area where the traverses were collected, showing the location of the blocks in the Campsite Dyke and the sample traverses collected as part of this study. Re-drawn from Irvine et al. (1998). The white cross-cutting dykes are camptonitic.

north of Homestead Bay, close to the Skaergaard Peninsula, where the lower part of UZ forms the host rocks (Fig. 2). This area, which has become informally known as the "campsite area", was mapped in detail by L.R. Wager during the 1935–6 expedition, and the map was later published by Vincent (1953). Wager also collected samples from all the exposed dykes in the region of Homestead Bay (currently housed in the Oxford Museum of Natural History). A more detailed map of the campsite area was published by Irvine et al. (1998), showing the cross-cutting relationships of the two dyke generations (Fig. 2b).

The present study is focused on the earlier, north–south trending, generation of dykes, thought to be closely related to the Skaergaard Intrusion (Brooks and Nielsen, 1978) and intruded shortly after its solidification. The campsite area contains two well-exposed dykes from this generation. One is a 6 m wide composite dyke, with an outer part, 60 cm thick on each side, chilled against the host, and an inner part with a chilled margin against the outer. This composite dyke, known as the Campsite Dyke (Jakobsen et al., 2010, following Irvine et al., 1998), has been traced southwards into UZb (Figs. 1, 2a) and northwards to Kraemer Island. It is notable for a localised concentration of large xenoliths (Figs. 1 and 2b). The most prominent and abundant of these xenoliths are gabbroic troctolite orthocumulates, although olivine gabbros and small fragments of basalt and sedimentary rocks are present (Irvine et al., 1998). On the basis of microstructure, mineralogy and the compositions of melt inclusions, Jakobsen et al. (2010) suggested that the most abundant type of xenolith – the gabbroic troctolites of Irvine et al. (1998) – may have been derived from the Skaergaard HZ. The other dyke, 6.5 m wide, contains numerous cm-scale phenocrysts of plagioclase notable for their abundant melt inclusions: we will refer to it as the Plagioclase-phyric Dyke. The relative age of the two dykes cannot be determined from field relations as no cross-cutting relationships are exposed (Irvine et al., 1998. Fig. 2b). Irvine et al. (1998) favoured the hypothesis that the Plagioclase-phyric Dyke is the older of the two.

3. Samples

For each of the Campsite and Plagioclase-phyric dykes, three samples were collected along a traverse from the margin to the centre, perpendicular to the dyke margins (Fig. 2b), close to the North House foundation where both dykes are 6–7 m wide. These samples were supplemented by a sample of the outer chilled zone of the Campsite Dyke, collected by Kent Brooks, together with samples collected by L.R. Wager from both the Campsite and Plagioclase-phyric dykes (part

of the collections of the Oxford University Museum of Natural History) (sample locations and numbers shown in Fig. 2a). While the exact position within each of the two dykes is not known for the Wager samples, the three-grain junction geometries in the groundmass are constant across each dyke, apart from the chill zone, and so the absence of detailed spatial information does not pose a problem for the present study. We do not have a sample of the chilled margin of the Plagioclase-phyric Dyke.

This set of samples of the two wide, N-S trending dykes was supplemented by a relatively basaltic example of the late E/W trending ALK-2 dykes (sample EG 4105, from the Oxford University Museum of Natural History. See Fig. 2a for location). We also collected a suite of samples from 8 randomly chosen gabbroic troctolitic xenoliths from the Campsite Dyke, ensuring that each sample was collected from the centre of the exposed surface of each block.

For comparison of the xenoliths with material from a currently active volcanic system, we examined a suite of glassy crystalline nodules from Iceland. Saxi and Fontur are large tuff cones in the northern part of the Veiðivötn–Vatnaöldur fissure system, and have been proposed as candidates for the source of the giant, 8600-year old (Hjartarson, 1988), Þjórsá basaltic flow (Hansen and Grönvold, 2000; Thordarson et al., 2003). Both cones rise only a few tens of metres from the surrounding plains and have well-developed central craters. They are composed predominantly of a glassy, poorly consolidated ash (Hansen and Grönvold, 2000), containing a mixture of volcanic bombs, fresh basaltic scoria, fragments of bright orange hyaloclastite (possibly country rock), and abundant sub-rounded gabbroic nodules. The nodules vary in size (10–100 mm in length), grain size (<0.5 mm overall to >10 mm for mono-crystalline feldspars), and modal mineral proportions. There is little or no variation in grain size towards their margins. The microstructures in the nodules have previously been described by Holness et al. (2007b).

4. Constraints on cooling rates

4.1. 1 Minor mafic intrusions

The first step in developing sufficient understanding of the two major N/S trending dykes in the campsite area is to establish not only their age relative to each other, but also their likely age relative to the Skaergaard Intrusion. The absence of evidence from cross-cutting relationships and the presence of chilled margins on both dykes mean that any method for determining their relative age must be independent of field observations. The particular case of minor intrusions cutting an earlier intrusion provides a situation in which dykes are intruded into a host that is gradually cooling. The earliest dykes intrude a hot host and will therefore cool more slowly than later dykes that intruded when the host was cold. It is therefore possible to construct a sequence of relative ages using a method based on interpretation of microstructural features that are controlled by cooling rate.

Crystal size distributions are commonly used to constrain the time over which solidification occurred (e.g. Cashman, 1993), but this approach is dependent on tight constraints on crystal growth rates (Holness et al., 2012b). However, it is possible to differentiate between rapidly-cooled from slow-cooled dykes of similar size, composition and phenocryst load from a simple consideration of the groundmass grain size. Thus, all other things being equal, a dyke intruding a hot host will be coarser-grained than a dyke that intruded later when the host was cold.

Perhaps the most obvious manifestation of the relative temperatures of host and intruding magma is the chilled margin. There will be no chill zone if the host rock was at the same temperature as the intruding magma, and the chill will become better developed and more fine-grained as the temperature difference between host and dyke increases. Although this distinguishing feature may be unreliable in the field if all dykes in the series have chilled margins, a close examination of the chills with an optical microscope may reveal a greater extent of subsolidus microstructural modification in chills formed with a relatively small temperature difference between the host rock and the intrusion. This is because the fine-grained chill will have had greater opportunity for textural equilibration in the sub-solidus as the heat from the inner parts of the dyke pass through it (c.f. Holness et al., 2012a, b).

A further method to constrain cooling rates is based on the geometry of three-grain junctions. Recent work has shown that the median value of the augite–plagioclase–plagioclase dihedral angle in dolerite sills, Θ_{cpp}, is a function of the crystallisation time if this is greater than ~10 years (Holness et al., 2012b). This observation provides us with the opportunity not only to distinguish between dykes intruding a cooling host at different times, but also to constrain the absolute timing of dyke intrusion relative to the cooling of the host.

For dolerites and basalts that took $\ll$10 years to solidify, augite–plagioclase–plagioclase three-grain junctions are formed by the intersection of planar augite–plagioclase grain boundaries, with grain boundary orientations determined by the random impingement of planar-sided plagioclase grains (Fig. 3a). However the population of augite–plagioclase–plagioclase dihedral angles is not exactly the same as the earlier population of melt-plagioclase–plagioclase angles (which has a median value of 60°), because the narrower melt-filled pores, formed by the impingement of plagioclase grains at a low angle, tend not to be filled by augite during rapid solidification. This is both because the glass transition temperature is encountered before the supersaturation reaches that required to grow augite into small spaces (e.g. Holness et al., 2012a), and because of the constraints placed on mass transport at low permeability. As a consequence 78° appears to be the general lower limit for Θ_{cpp} in rapidly cooled dolerites.

Dolerites that took longer than ~10 years to crystallise develop curvature of augite–plagioclase grain boundaries close to three-grain junctions (Fig. 3b). This curvature results in higher Θ_{cpp}, with values reaching ~100° in the centre of thick (~300 m) sills (Holness et al., 2012b). The development of curvature is thought to be a consequence of the changing balance between the growth rates of augite and plagioclase during the final stages of crystallisation as each three-grain junction is formed: in rapidly-cooled rocks augite grows much faster than plagioclase during the formation of the three-grain junctions whereas in more slowly-cooled rocks augite and plagioclase growth rates are commensurate (Holness et al., 2012a).

The empirical relationship between Θ_{cpp} and crystallisation time developed by Holness et al. (2012b) is based on the assumptions of a far-field country rock temperature of 0 °C and a crystallisation interval of 1200–1000 °C. This approximation was suitable for the sills studied by Holness et al. (2012b) because these sills intruded relatively cold sedimentary rocks in the shallow crust. However, we can use this empirical relationship to test whether a dyke or sill of known width was emplaced into cold country rock. If, for a given dyke width and position within the dyke, Θ_{cpp} is higher than predicted from the Holness et al. (2012b) data, the country rock must have been sufficiently hotter than 0 °C to significantly retard cooling and crystallisation in the dyke. Thus a dyke emplaced into a very recently solidified layered intrusion will have a higher Θ_{cpp} than that expected for its width, whereas Θ_{cpp} in a dyke emplaced much later, once the host layered intrusion had cooled, will fall closer to, or on, the trend mapped by Holness et al. (2012b).

4.2. Cumulates

If the crystal growth rate is adequately well-known crystal size distributions can be used to determine cooling rates in mafic plutonic rocks. Care must be taken to account for the constraints on growth placed by grain impingement at high crystallinities (Schiavi et al., 2009), and the likelihood that nucleation of new grains will be inhibited

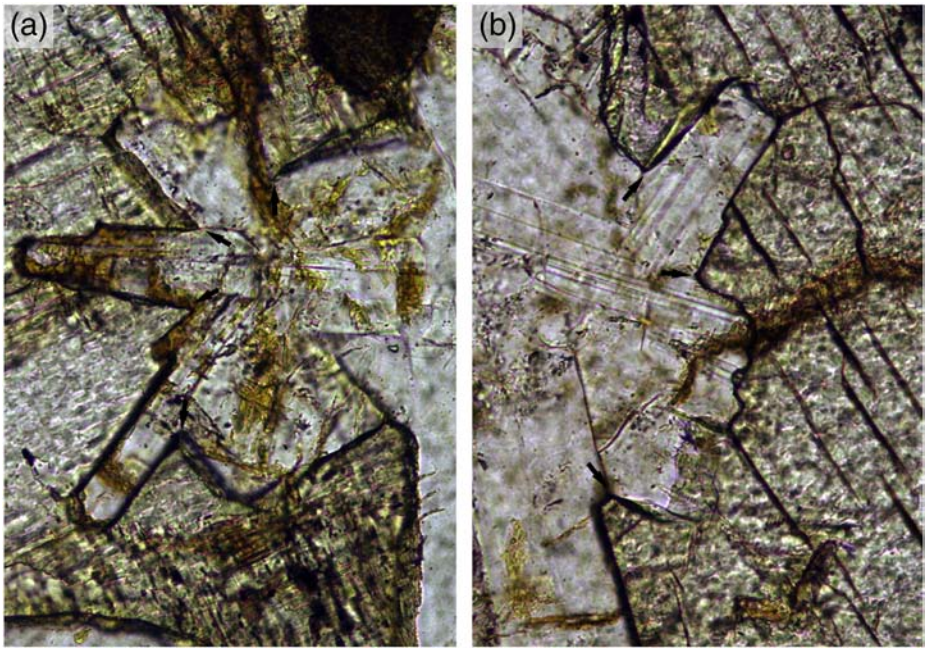

Fig. 3. Photomicrographs of doleritic microstructures. (a) Rapidly cooled dolerite in which augite–plagioclase–plagioclase three-grain junctions are formed by the intersection of planar augite–plagioclase grain boundaries (examples are arrowed). In the slower cooled example shown in (b) the augite–plagioclase grain boundaries are curved adjacent to the three-grain junctions, leading to higher dihedral angles (examples are arrowed). The differences in three-grain junction geometry are thought to be a consequence of changes in relative growth rates of the two minerals.

once pore sizes are reduced (e.g. Holness and Sawyer, 2008; Holness et al., 2012a). An elegant solution to these problems is to use poikilitic rocks in which early stages of crystal growth are preserved (e.g. Higgins, 1998).

Cooling times can be deduced from the width, crystallographic orientation, spacing and composition of exsolution lamellae in pyroxene grains (e.g. Brearley, 1991; Grove, 1982; McCallum and O'Brien, 1996). It may also be possible to place approximate qualitative constraints on cooling rates by considering whether or not pigeonite has inverted to hypersthene.

In contrast to dolerites, dihedral angle populations in mafic cumulates are not straightforward to interpret. In progressively fractionated layered intrusions, Θ_{cpp} remains constant over large stretches of stratigraphy, with step-wise changes associated with the addition or subtraction of phases from the liquidus assemblage of the bulk magma (Holness et al., in press). Although there appears to be some control by cooling rate, via the control on fractional latent heat exerted by the enthalpy budget (Morse, 2011), we do not currently have a simple empirical relationship linking cooling rate and Θ_{cpp}. However, in the specific case of the troctolitic xenoliths in the Campsite Dyke, we can make direct comparisons between Θ_{cpp} measured in the xenoliths and published values for the troctolitic parts of the Layered Series (HZ and LZa) (Holness et al., 2007a,c, in press).

5. Analytical techniques

Dihedral angles were measured using a Leitz 4-axis universal stage mounted on a James Swift monocular microscope fitted with a UM32 Leitz long-working-distance objective. Populations of up to 100 individual measurements of true dihedral angles (i.e. with the grain boundaries oriented parallel to the direction of view) were made on each sample, with the 95% confidence intervals about the median calculated according to the method of Stickels and Hücke (1964).

Plagioclase grain size was obtained by measuring the long axis of all plagioclase grains in photomicrographs at a sufficient magnification to ensure all grains were visible. Between 200 and 400 grains were measured for the groundmass in each sample (avoiding phenocrysts) and a simple average was taken to be an adequate measure of grain size for comparative purposes.

Mineral compositions were obtained with a Cameca SX-100 electron microprobe (EPMA) at the University of Cambridge. A15kV and 10 nA beam were used with a spot size of 1 μm. Peak counting times were 20s for major elements and 40s for minor elements. Some line profiles were analysed for plagioclase. Line profiles, with spots spaced every 2 μm, were analysed for both augite and pigeonite to obtain average analyses of bulk grains where exsolution was visible. The following standards were used for Kα X-ray lines calibration: diopside for Si and Ca; rutile for Ti; corundum for Al; spessartine for Mn; fayalite for Fe; periclase for Mg; jadeite for Na; K feldspar for K; NiO for Ni; and Cr for Cr. Crystals used in spectrometers were TAP for Si, Ti, Al and Mg; PET for Ca, Na and K and LIF for Mn, Fe, Cr and Ni. Raw data were corrected with the CITZAF software.

Mineralogical X-ray mapping was carried out with the QEMSCAN® 4300 at Camborne School of Mines, University of Exeter. The instrument is a Zeiss EVO50 scanning electron microscope equipped with four Bruker X-flash energy dispersive X-ray detectors, automated electron beam and specimen stage control, X-ray spectrum acquisition and classification. For each sample, 5 to 7 million X-ray spectra were collected at 1000 X-ray counts in a 10 μm raster grid on the thin section surface (fieldscans, Gottlieb et al., 2000; Pirrie et al., 2004), matched to a spectral database (a customised species identification protocol based on the Intellection LCU5 database), and assigned to compositional (mineralogical) groups. Feldspar zoning was resolved using the relative signal heights of Si-Kα and Ca-Kα.

6. Microstructures of the dykes

6.1. Campsite Dyke

The outermost chill zone of the Campsite Dyke contains clots of euhedral plagioclase and fresh olivine phenocrysts (Fig. 4a) set in a fine-grained matrix of euhedral plagioclase, rounded aggregates of pyroxene and irregular patches of Fe–Ti oxides (Fig. 4b). Some euhedral phenocrysts (?olivine) are completely replaced by fine-grained sheet

silicate minerals (Fig. 4a). Although we did not measure Θ_{cpp}, high-resolution back-scatter electron images show that there has been significant modification of the primary igneous microstructure, with rounding of grain boundaries and an increase in the dihedral angle at augite–plagioclase–plagioclase junctions (Fig. 4c).

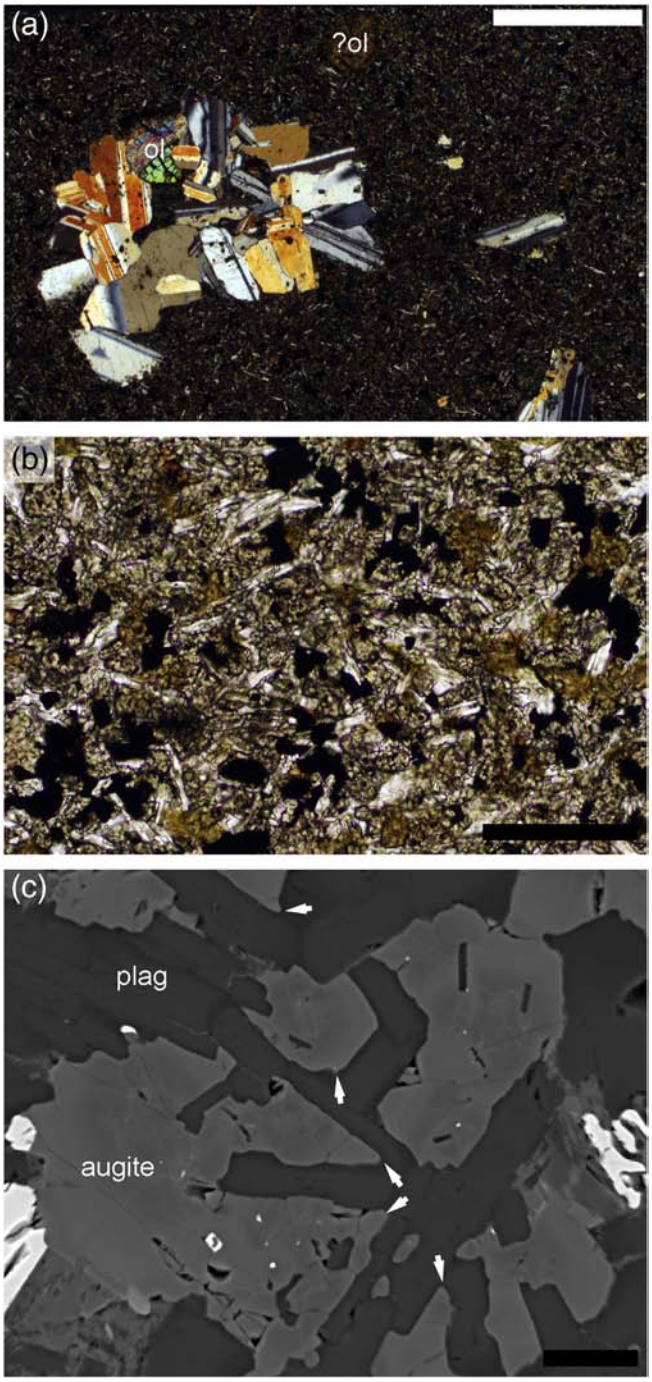

Fig. 4. The outer chill zone of the Campsite Dyke. (a) Crystal clots and isolated phenocrysts of plagioclase and olivine are common, together with completely replaced phenocrysts of ? olivine. Crossed polars. Scale bar is 1 mm long. (b) The fine-grained groundmass comprises plagioclase, pyroxene, Fe–Ti oxides and an altered mineral that might have been either olivine or orthopyroxene. Plane polarized light. Scale bar is 100 μm long. (c) Back-scatter electron image showing the normal zoning on all plagioclase grain margins. Note the rounded grain boundaries and the relatively high augite–plagioclase–plagioclase dihedral angles (examples are arrowed). This is consistent with significant sub-solidus textural modification of an initial quench microstructure. Scale bar is 20 μm long.

The inner chill zone (sample SKG11-11-11) begins 60 cm from the margin of the Campsite Dyke. It contains crystal clots and phenocrysts of plagioclase, augite and olivine (generally completely altered) in a micro-doleritic matrix (Fig. 5a). In the centre of the dyke the larger grain size of the matrix means the phenocrysts are no longer so apparent. The groundmass consists of coarse-grained plagioclase and augite, with skeletal oxides and some localised patches of completely altered material that may have originally been olivine (Fig. 5b). The three-grain junctions are slightly rounded (Fig. 5c). Θ_{cpp} in all five samples from the interior of the dyke is in the range 88–89.5° (Table 1). The grain size of the dyke increases from the margins inwards, with the average long axis of the plagioclase reaching a maximum of 0.41 mm (Table 1).

6.2. Plagioclase-phyric Dyke

We do not have a sample of the chill zone of this dyke. The microstructure in the centre of the dyke comprises a matrix of euhedral but altered olivine, elongate plagioclase, interstitial oxides and pyroxene. The dyke contains abundant plagioclase phenocrysts up to 2 cm long, with a preferred alignment parallel to the dyke margins. These phenocrysts contain abundant melt inclusions (Fig. 5d). Θ_{cpp} in all five samples from the interior of the dyke falls in the range 77.5–79° (Table 1). The grain size of the groundmass increases from the margin to the centre, with the average long axis of plagioclase reaching 0.24 mm (Table 1).

6.3. The E/W trending dyke

The single sample of the late generation of E/W trending ALK-2 dykes has a fine-grained doleritic microstructure. Θ_{cpp} is 79.5 ± 5° (Table 1).

7. Microstructures of xenoliths and nodules

The Skaergaard xenolith samples can be divided into two groups, primarily on the basis of microstructure. For this preliminary study we obtained electron microprobe analyses of five representative samples.

7.1. Gabbroic troctolites with variable degrees of partial melting — Type A

This group of five xenoliths (sample numbers SKG11-11-1, 2, 3, 7 and 8) comprises rocks dominated by Ca-rich pyroxene and plagioclase (Fig. 6a), with minor olivine and Fe–Ti oxides. Olivine grains where present (with variable extents of alteration) are isolated and commonly compact, indicating a primocryst origin. The plagioclase grains are elongate, denoting a primocryst origin, but commonly have irregular grain boundaries (Fig. 6b). Some may contain large irregular melt inclusions but the inclusions are not as numerous, large, or distinctive as those in the Type B xenoliths. They commonly have complex internal compositional zoning. Many grains, particularly where adjacent to pockets of interstitial oxides, biotite and apatite, have wide, constant-composition, normally zoned rims typical of the LZ of the Skaergaard Intrusion. These rims have been described by Namur et al. (submitted for publication) who suggest they formed during thermal buffering by crystallisation within the mushy layer (Figs. 6b, 7).

Type A xenoliths, with the exception of SKG11-11-1, contain primitive plagioclase: cores in the fine-grained sample SKG11-11-2 have compositions of $An_{78–84}$ with sodic rims of either constant composition at An_{45} or normally zoned down to An_{20}. In sample SKG11-11-8 the plagioclase core composition is $An_{78–82}$ with wide rims of constant composition of ~An_{65} or with normally zoned rims down to An_{45} (Table 2). In contrast, plagioclase core compositions in SKG11-11-1 are generally in the range $An_{58–60}$ although some grains are present with An_{52}. The anorthite content at the margins decreases over ~5–10 μm to form a wide sodic rim at ~An_{50} (Fig. 7).

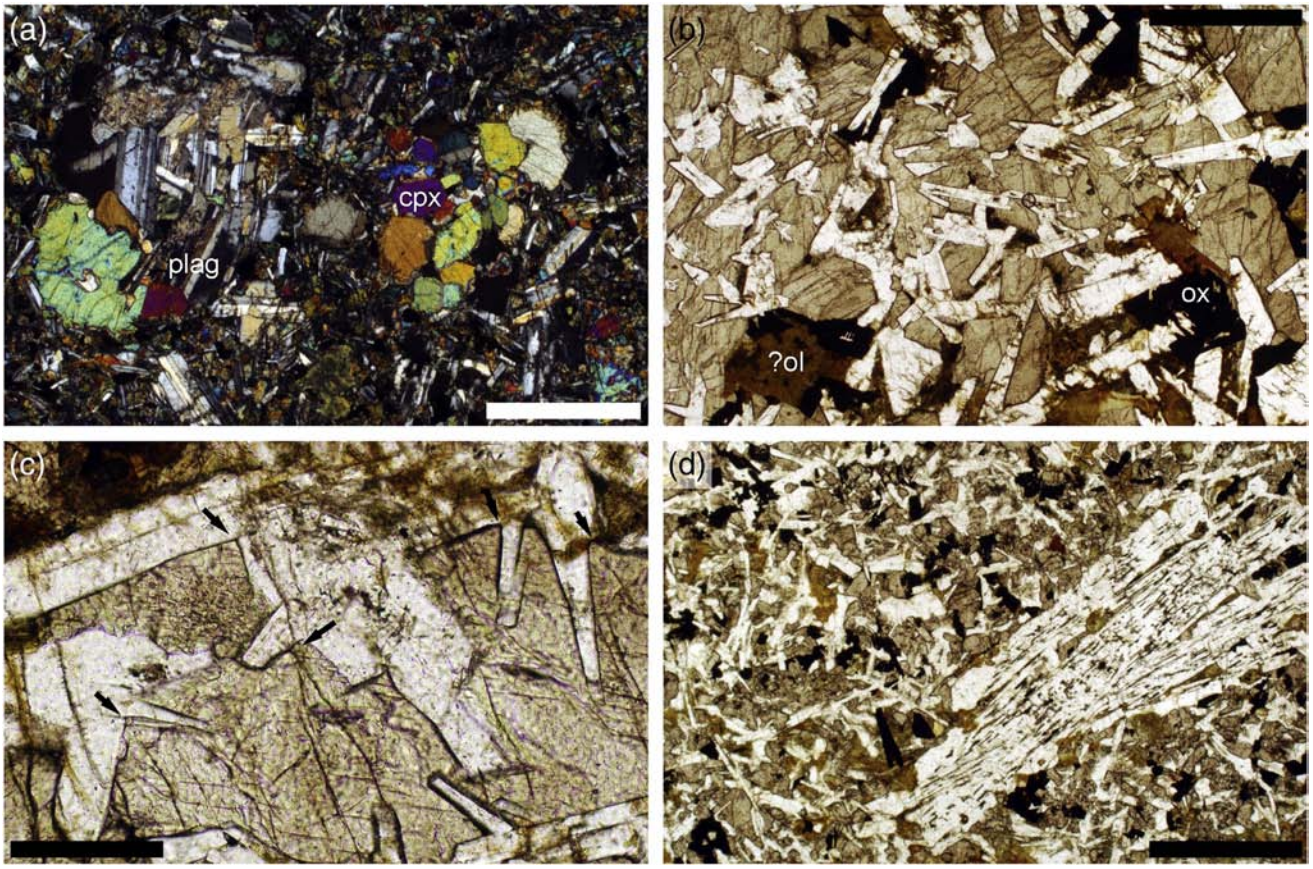

Fig. 5. The Campsite and Plagioclase-phyric dykes. (a) The inner chill zone of the Campsite Dyke contains abundant clots and phenocrysts of plagioclase and clinopyroxene set in a microdoleritic groundmass. Sample SKG11-11-11. Crossed polars. Scale bar is 1 mm long. (b) The interior of the Campsite Dyke (sample SKG11-11-12). Plagioclase is clear whereas augite is brown. Olivine is entirely replaced in the area shown, while Fe–Ti oxides grains have a skeletal habit. Plane polarized light. Scale bar is 1 mm long. (c) Sample SKG11-11-12 from the centre of the Campsite Dyke. Note the rounded grain boundaries forming relatively high augite–plagioclase–plagioclase dihedral angles (examples are arrowed). Plane polarized light. Scale bar is 200 μm long. (d) The central part of the Plagioclase-phyric Dyke (sample SKG11-48A) showing a cluster of large plagioclase phenocrysts, each with abundant melt inclusions. Plane polarized light. Scale bar is 1 mm long.

In all Type A xenoliths augite, although modally dominant, is always interstitial, commonly with a poikilitic habit. Augite in the four relatively primitive samples contains no exsolution lamellae visible with a scanning electron microscope, and has Mg numbers between 75 and 83 (atomic percent). No low-Ca pyroxene is present in this group. In contrast, the relatively evolved sample SKG11-11-1 contains augite with exsolution lamellae of Ca-poor pyroxene (Fig. 8). The lamellae form two generations, one 0.5–0.75 μm wide and the other ~0.1 μm wide. This sample also contains partially inverted interstitial pigeonite (Fig. 6c). The pigeonite contains wide, parallel-sided exsolution lamellae of augite close (but not strictly parallel) to the host (100) planes. The exsolution lamellae form two generations, with a widely-spaced set 4–5 μm wide (generally containing thin and discontinuous low-Ca pyroxene lamellae at a

Table 1
Microstructural data for the dykes. The number of individual dihedral angle measurements in each sample is given by n, Θ_{cpp} is the median of the population, and St. deviation is the standard deviation. The 2 σ uncertainties on Θ_{cpp} are calculated according to the method of Stickels and Hücke (1964). Average grain size gives the average length of the long axis of plagioclase grains in mm.

Sample	Distance from margin (m)	n	Θ_{cpp}	St. deviation	Average grain-size (mm)
Campsite Dyke — 6 m wide					
SKG11-11-11	0.60	100	88 ± 3.5°	16.7°	0.12
SKG11-11-12	1.90	100	89 ± 2.5°	14.1°	0.30
SKG11-11-10	2.95	100	89.5 ± 5°	18.6°	0.41
EG 2577	–	70	89 ± 3°	15.4°	–
EG 4279	–	40	89 ± 4°	13.6°	–
Plagioclase-phyric Dyke — 6.5 m wide					
SKG11-48A	1.30	100	78 ± 3°	15.2°	0.15
SKG11-49A	2.60	100	79 ± 3°	17.5°	0.20
SKG11-50A	3.70	100	79.5 ± 3°	19.8°	0.24
EG 4266	–	100	77.5 ± 4.5°	20.3°	–
EG 4261	–	50	79 ± 4.5°	16.7°	–
Late E/W trending dyke					
EG 4105	–	50	79.5 ± 5°	24.0°	–

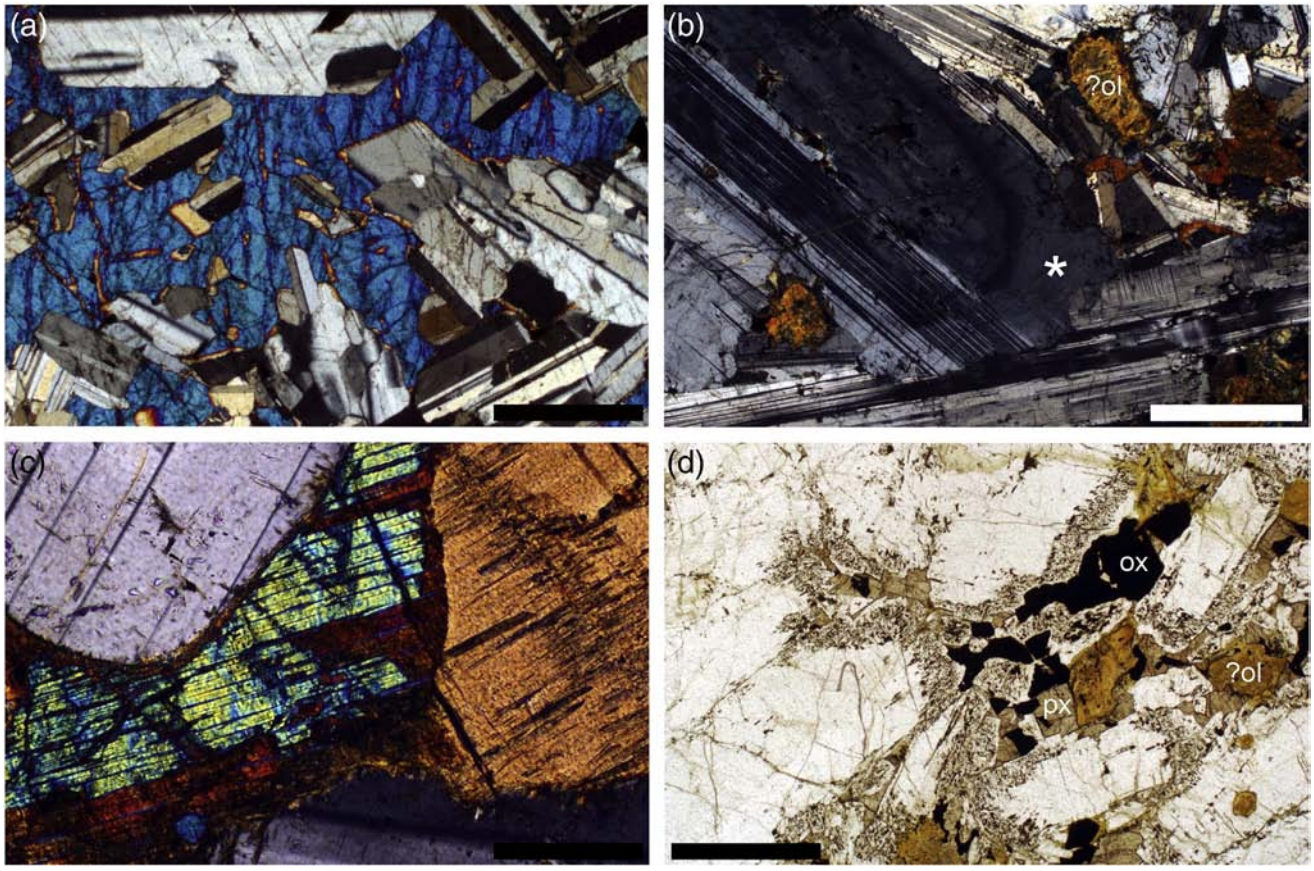

Fig. 6. Type A xenoliths from the Campsite Dyke. (a) Sample SKG11-11-8 is dominated by primocrysts of plagioclase, with interstitial augite of homogeneous composition (no exsolution lamellae are visible, even under SEM). Crossed polars. Scale bar is 1 mm long. (b) Sample SKG11-11-3. Note the wide range of plagioclase grain size. The largest grain in the field of view has a thick rim of constant composition (marked with an asterisk). Crossed polars. Scale bar is 1 mm long. (c) Sample SKG11-11-1. The pyroxene grain on the left is partially inverted pigeonite. The blue birefringent part of the grain is pigeonite whereas the reddish part is inverted. Note the wide and planar-sided exsolution lamellae. The pyroxene grain on the right is augite, with much thinner exsolution lamellae of Ca-poor pyroxene (not visible in this image). Crossed polars. Scale bar is 200 μm long. (d) Sample SKG11-11-3. Olivine primocrysts (?ol) in this field of view are completely replaced by sheet silicates. Interstitial augite (px) and Fe–Ti oxides (ox) are surrounded by plagioclase (clear) which is scattered with abundant melt inclusions. This part of the rock crystallised at relatively low temperature and so was the first to melt on entrainment in the dyke. Plane polarized light. Scale bar is 1 mm long.

slightly different orientation to the host augite lamella), and a more closely-spaced set <0.5 μm wide (Fig. 8). Average analyses of the augite provide bulk compositions with Mg numbers of 63–66 (average 64), while the bulk pigeonite composition is $Wo_{10.5}En_{49}Fs_{41.5}$.

Minor interstitial phases include Fe–Ti oxides, biotite and (euhedral) apatite. Some samples contain pockets of coarse-grained granophyre bounded by planar-sided plagioclase primocrysts (Fig. 7). Three of the five Type A xenoliths (SKG11-11-3, 7 and 8) have been partially melted, with melting concentrated in the wide, constant-composition, rims of the plagioclase grains surrounding grains of interstitial Fe–Ti oxides (Fig. 6d). Dihedral angles could not be measured in these partially melted samples.

7.2. Gabbroic troctolites with melt inclusion-rich plagioclase — Type B

This group (sample numbers SKG11-11-4, 5 and 6) comprises xenoliths similar to those that were the focus of the study by Jakobsen et al. (2010). The three samples are coarser-grained than Type A xenoliths (Fig. 9). Plagioclase grain size is generally bimodal and the larger primocrysts are filled with large and abundant melt inclusions (now crystalline). The plagioclase walls of the melt inclusions are sodic (Jakobsen et al., 2010). The large plagioclase grains are elongate, with rounded ends and irregular margins (Fig. 10a). The cores of the plagioclase grains in SKG11-11-4 are ~An_{70}, and in SKG11-11-5 are $An_{81–83}$. The thick rims of constant composition that are typical of Type A xenoliths are locally present but are very rare. Instead the plagioclase has either no rims, or rims with a sharp inner margin marked by a drop in An content by 10–20 mol%, followed by a constant and smooth decline in anorthite content to a marginal value of ~An_{45}. Olivine forms variably altered, rounded, subhedral grains that are interpreted as primocrysts. Augite is interstitial and is compositionally uniform (Mg number 66–70 (SKG11-11-4) and 79–83 (SKG11-11-5)), with no exsolution lamellae visible under the scanning electron microscope.

Augite and melt-inclusion rich plagioclase grains are commonly intergrown, with elongate apophyses of augite penetrating individual plagioclase grains (Fig. 10b), and filling, either partially or completely, some of the melt inclusions (Fig. 10c), as though the plagioclase grain had contained irregular melt-filled holes and tubes, some of which were filled with augite. Augite fills the spaces between the rounded ends of the large irregular plagioclase grains, resulting in a highly irregular shape for these interstitial grains. Plagioclase immediately adjacent to the intergrown augite, both on grain boundaries and around the filled melt inclusions, is sodic, with a sharply defined inner margin to the sodic rim (Fig. 10d).

7.3. Icelandic glassy nodules

The glassy gabbroic nodules of relevance to this study are all highly crystalline, with <20 vol.% vesicular glass. The nodules are dominated by randomly oriented, rounded, plagioclase grains with irregular

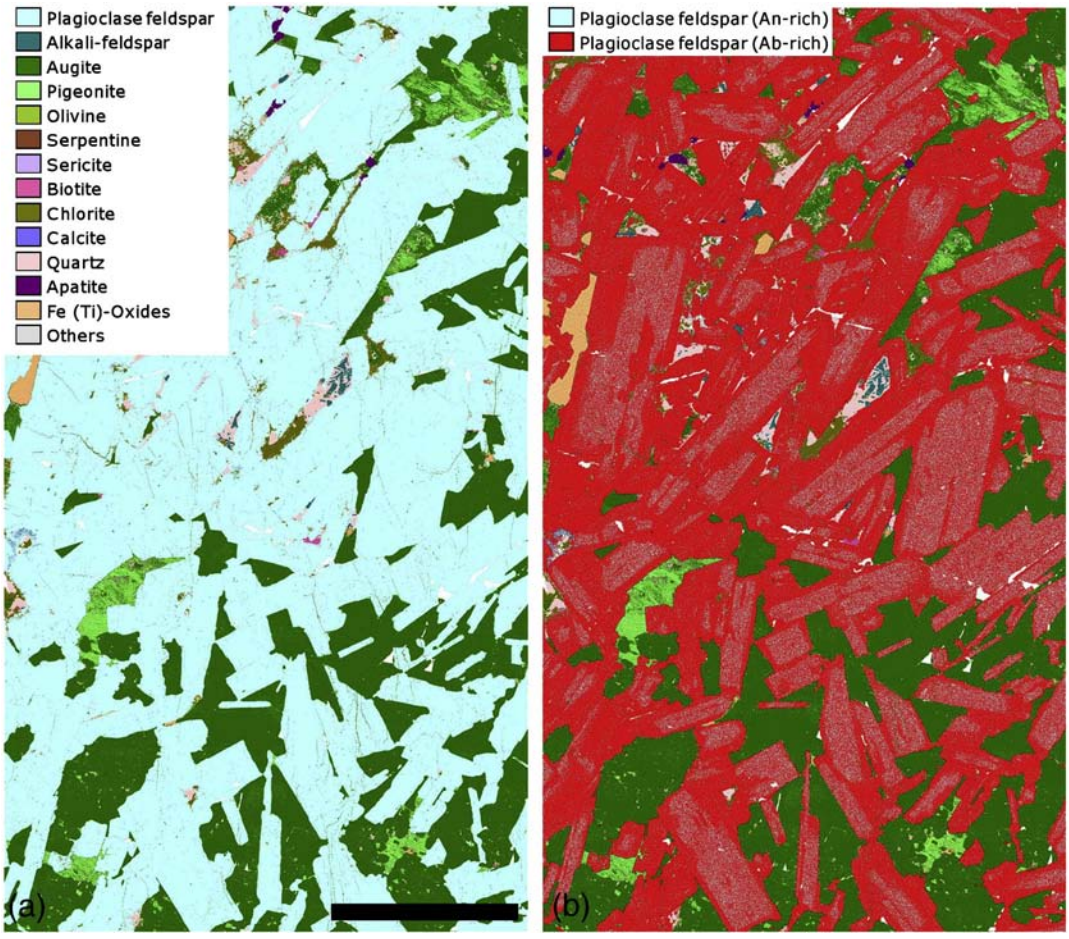

Fig. 7. QEMSCAN images of xenolith SKG11-11-1. (a) A map of mineral distribution. Note the triangular pockets of granophyre. (b) A map in which the plagioclase has been differentiated depending on composition. Note the wide albitic rims on almost all grains. These are thought to form during thermal buffering of the mushy layer, triggered by nucleation and growth of interstitial augite (Namur et al., submitted for publication). Scale bar is 5 mm long.

margins (Fig. 11a, b). The plagioclase grains contain abundant irregularly shaped melt inclusions that are generally filled with glass (Fig. 11a, b), although some contain augite (Fig. 11c, d). The plagioclase rims of the augite-filled inclusions are sodic (Fig. 11c, d). Primocrysts of olivine (together with augite in some nodules) have well-developed grain boundaries with the adjacent plagioclase (Fig. 11b, e). Many three-grain junctions involving either olivine or augite and two grains of plagioclase are not completely formed, with a pocket of glass at the junction. This is most common for olivine, whereas augite may grow as small interstitial grains, filling the previously melt-filled space with a low augite–plagioclase–plagioclase dihedral angle (Fig. 11e). Augite commonly forms interstitial grains within the melt films separating plagioclase primocrysts: the rounded and irregular margins of the plagioclase primocrysts give this interstitial augite a highly irregular appearance (Fig. 11b).

The larger melt pockets in the nodules contain rounded symplectic intergrowths of augite and elongate plagioclase, commonly with a radiating arrangement of the plagioclase (Fig. 11a). Plagioclase primocrysts commonly have a sodic rim and the margins of all primocryst phases, where in contact with large melt pools, commonly display a cellular interface or dendritic morphology. The margins of both augite and plagioclase primocrysts may be in optical continuity with augite–plagioclase symplectites in the melt pool (Fig. 11f).

Table 2
Microstructural and compositional data for the xenoliths in the Campsite Dyke. The number of individual dihedral angle measurements in each sample is given by n, Θ_{cpp} is the median of the population, and St. deviation is the standard deviation. The 2 σ uncertainties on Θ_{cpp} are calculated according to the method of Stickels and Hücke (1964). The compositions of the centres of plagioclase, olivine and augite primocrysts are indicated. The Jakobsen et al. (2010) average compositional data are reported for comparison under the heading Type B.

Sample	n	Θ_{cpp}	St. deviation	Plagioclase (An mol.%).	Olivine (Fo mol.%)	Augite (Mg#)
Type A						
SKG11-11-1	40	95.5 ± 4°	12.7	58–60	–	64
SKG11-11-2	50	80 ± 6°	21.1	78–82	76–78	77
SKG11-11-8	50	86 ± 4°	11.3	80–83	–	81
Type B						
Jakobsen et al.	–	–	–	79–82	80	81
SKG11-11-5	30	80.5 ± 6°	26.0	79–83	–	83
SKG11-11-4	50	79.5 ± 10°	22.4	66–70	74–75	75

8. Thermal modelling

The temperature of the UZb cumulate rocks forming the country rock (at the southern end of the dyke outcrop, Fig. 2a) at the time of intrusion must have been sufficiently cool to have permitted brittle failure, and they were therefore likely to have been completely, or almost completely, solid. The liquidus temperature of the bulk liquid that formed the Sandwich Horizon was ~1000 °C (Thy et al., 2009) and, given that the interstitial liquid in the UZb cumulates is likely to have had a composition similar to that of the bulk liquid at the Sandwich Horizon, this is a plausible temperature for complete solidification of

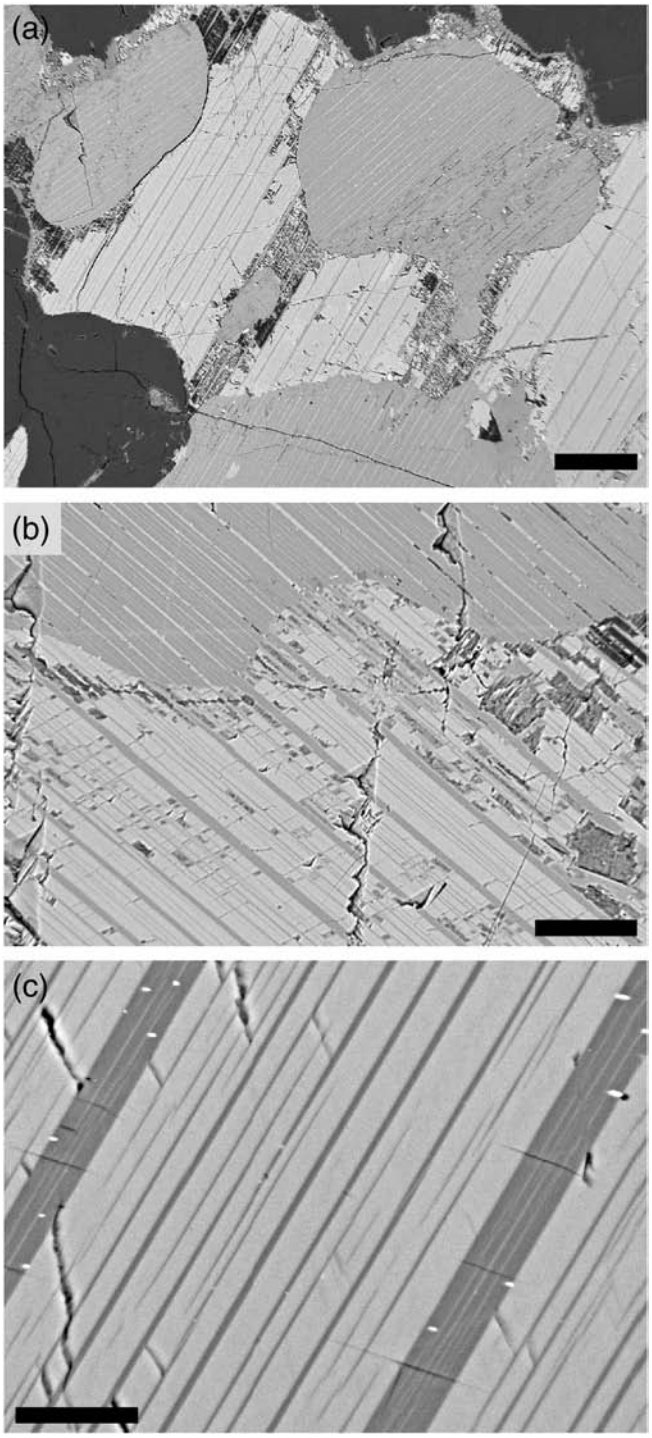

Fig. 8. BSE images of pyroxenes in sample SKG11-11-1. (a) Intergrown primocrysts of Ca-rich (mid-grey) and low-Ca (pale grey) pyroxene (pigeonite), both of which exhibit exsolution lamellae, together with plagioclase (dark grey). The low-Ca pyroxene contains abundant patches of small pits — these are altered to sheet-silicates. Scale bar is 100 μm long. (b) The boundary between two grains of pyroxene, one Ca-rich augite (top) and the other Ca-poor pigeonite (bottom). Note the similarity of orientation of the exsolution lamellae (assumed to be parallel to (001) in both grains), suggesting of a topotactic relationship during nucleation and growth. The exsolution lamellae in the Ca-poor pyroxene are generally much wider than those in the Ca-rich pyroxene. Note the discontinuous {110} cleavage cracks in the pigeonite grain. Scale bar is 20 μm long. (c) Close-up of exsolution lamellae in pigeonite. Note the presence of relatively wide lamellae with much thinner lamellae between. The wide lamellae of Ca-rich pyroxene themselves contain a further generation of Ca-poor exsolution lamellae. The bright spots are most probably ilmenite blebs exsolved from the augite lamellae. Scale bar is 10 μm long.

UZb. The upper bound on the country rock temperature is that of the liquidus of the bulk magma in UZb. While there is considerable disagreement concerning the liquidus temperatures of the progressively evolving Skaergaard magma, Thy et al. (2009) place the arrival of cumulate apatite at 1050 °C, broadly in agreement with Morse et al. (1980) but considerably lower than Morse (2008), McBirney and Naslund (1990), Kudo and Weill (1970) and Williams (1971) who all advocate temperatures of ~1100 °C.

The composition of the Campsite Dyke chill zone given by Jakobsen et al. (2010) has a liquidus at 1190 °C calculated using the MELTS programme (Ghiorso and Sack, 1995) at 3.5 kbar (Larsen and Tegner, 2006). All feldspar and clinopyroxene are fully crystallised by 1000 °C. We therefore assume a crystallisation interval of 1200–1000 °C.

The cooling time from 1200 °C to 1000 °C was calculated in one dimension for a 6.5 m wide dyke-like intrusion, initially at 1200 °C, instantaneously injected into a background environment of constant temperature. Heat transport was assumed to be only by thermal diffusion, with a thermal diffusivity of 31.5 m^2/yr. Inside the intrusion, the latent heat of the magma was assumed to be released uniformly over the cooling interval, with a ratio of latent heat to specific heat (L/C_p) of 500 K. From a dimensional argument, the cooling time for wider or narrower dykes can be inferred as being proportional to the square of the dyke thickness. Hence a 13 m wide dyke cools 4 times more slowly than a 6.5 m wide dyke. The times to crystallise 3 dykes, of 3.25 m, 6.5 m and 13 m thickness are shown as a function of country rock temperature in Fig. 12.

9. Discussion

9.1. The relative and absolute ages of the Campsite and Plagioclase-phyric dykes

If we assume that the phenocryst load of the Plagioclase-phyric Dyke did not affect the grain size of the groundmass, the relatively coarse grain size of the groundmass in the Campsite Dyke compared to the Plagioclase-phyric Dyke (Table 1) points to the Campsite Dyke being the older of the two. However, without accurate knowledge of the rate of plagioclase growth we cannot pinpoint the temperature of the host. For this we need to turn to the observed values of Θ_{cpp} which can be mapped onto expected duration of crystallisation using the empirical relationship obtained by Holness et al. (2012b).

The higher values of Θ_{cpp} in the Campsite Dyke require cooling times of the order 15–74 years (using the 95% confidence intervals to obtain lower and upper bounds for Θ_{cpp} of 85° and 91° respectively, together with the best fit line through the Holness et al. (2012b) data), whereas the upper bound for Θ_{cpp} of 81° in the Plagioclase-phyric Dyke leads to a maximum crystallisation time of ~1 year. The value of Θ_{cpp} in the late cross-cutting E/W dyke is indistinguishable from that of the expected minimum value for very rapidly-cooled magma (Table 1) consistent with this generation of dykes having intruded late into a cold host. The timescales obtained for the Campsite and Plagioclase-phyric Dykes can be used to determine the country rock temperature necessary to generate the required cooling rates (assuming that the country rock remains at constant temperature for the duration of dyke solidification, a reasonable assumption given the relative sizes of the dykes and the Skaergaard Intrusion).

The ranges of probable crystallisation times are shown in Fig. 12 and suggest that the UZ cumulates had cooled to temperatures of 920–970 °C before the Campsite Dyke intruded, whereas they had cooled substantially more, below 670 °C, at the time the Plagioclase-phyric Dyke intruded. The Campsite Dyke is thus the older of the two (confirming the initial conclusion based on grain size), and intruded shortly after solidification of the Layered Series.

The chill zone on the Campsite Dyke developed despite a difference in temperature between the magma and the host rock of only about 250 °C. However, the relatively high temperature of the country rock

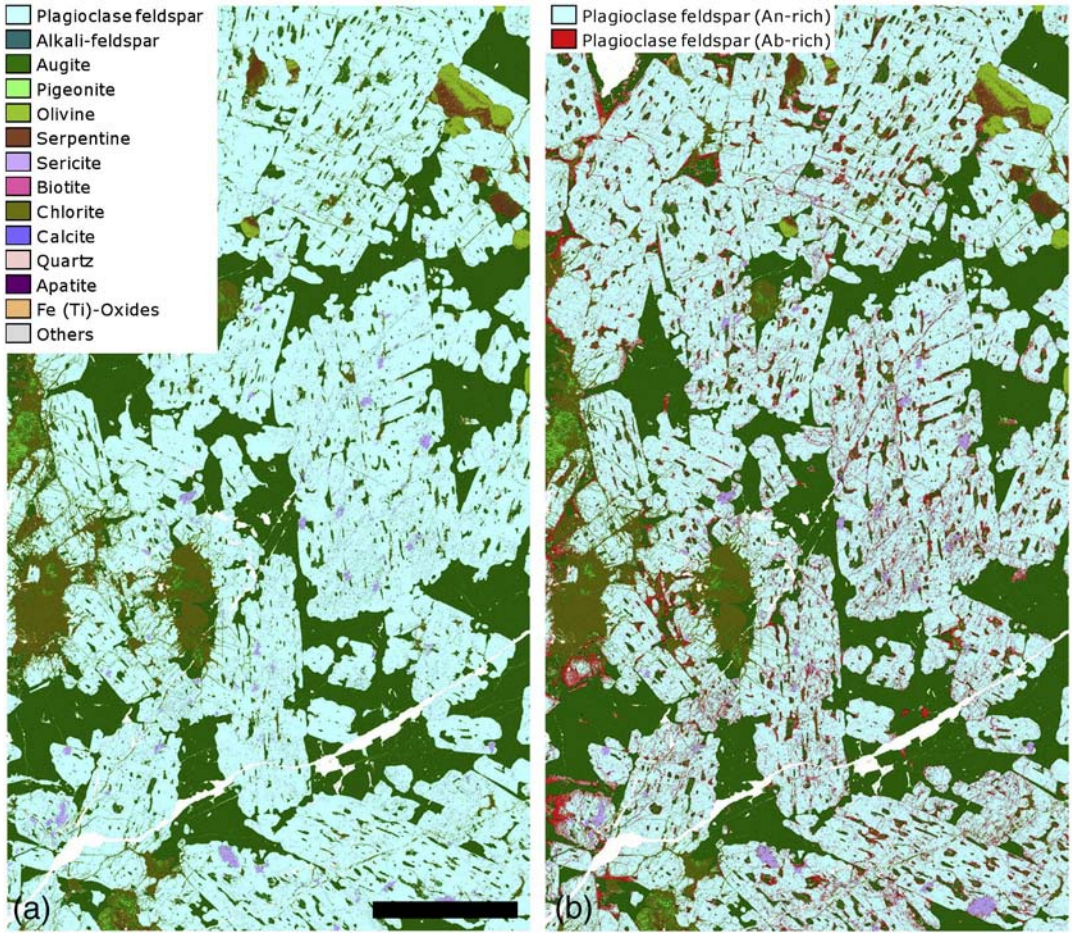

Fig. 9. QEMSCAN images of xenolith SKG11-11-5. (a) A map of mineral distribution. (b) A map in which the plagioclase has been differentiated depending on composition. The thick rims characteristic of SKG11-11-1 (Fig. 7b) are not present. Instead there are minor patches of albitic plagioclase associated with the abundant melt inclusions in the plagioclase and in localised pockets on grain boundaries. Scale bar is 5 mm long.

resulted in significant sub-solidus modification of the chill zone of the Campsite Dyke, with an approach to a granular microstructure and an increase in dihedral angle (Fig. 4c). We anticipate that the microstructure throughout the Plagioclase-phyric Dyke is unmodified from the original igneous microstructure.

9.2. Comparison of the xenolith blocks with the Skaergaard Layered Series

Type A xenoliths have microstructures very similar to those of the lower parts of the Layered Series. The interstitial status of the oxide minerals points to an affinity with cumulates below LZc. The most evolved of this group, SKG11-11-1, contains plagioclase with compositions that, by comparison with compositions at the LZa/b boundary (Maaløe, 1976) are consistent with a source in the lower part of LZb. The An_{50} composition of the thick rims is also consistent with a source in LZb (Namur et al., submitted for publication). This suggests that the augite in this xenolith is actually cumulus, rather than entirely interstitial, in agreement with other studies that have described a gradual progression towards granular augite at the LZa/b transition (e.g. Holness et al., 2007a). The average bulk augite Mg number of 64 is considerably lower than the value of 68 obtained for a mid-LZ sample (sample number 4389: Nwe, 1976) but the same as that obtained for a MZ gabbro (Nwe, 1976). However, the range of variability of augite composition and the extent of metastability (e.g. Morse, 2001) are not well known for the Skaergaard so the significance of these observations cannot yet be evaluated. The final microstructural evidence supporting a source in LZb is that $\Theta_{cpp} = 95.5 \pm 4°$. This value is within error of that expected for LZb (Fig. 13).

The bulk compositions for the co-existing augite and pigeonite in SKG11-11-1 result in temperatures of 1015–1053 °C using the QUILF thermometer (Andersen et al., 1993). This range is much lower than the ~1100 °C expected for the LZ liquidus (Thy et al., 2009) suggesting either that the averaged pyroxene compositions are not representative or that there was significant inter-grain Mg–Fe diffusion prior to the development of the exsolution lamellae. Although we sought to include a statistically significant number of exsolution lamellae in our averaged composition we may have missed blebs of more granular exsolution (e.g. Lindsley and Andersen, 1983), resulting in a less sub-calcic composition for the augite.

The remainder of the Type A xenoliths has more primitive plagioclase and augite. While the most primitive compositions from the exposed parts of the intrusion are found in the MBS, with plagioclase of An_{72} and olivine with Fo_{84} (Hoover, 1989), the most primitive compositions from the Layered Series are found at the base of the Cambridge drill core, with plagioclase of ~An_{70} (Maaløe, 1976) and olivine with Fo_{65} (Nwe, 1976). The plagioclase composition is considerably more evolved in both available examples of primitive Skaergaard cumulates than that in SKG11-11-2 and 8 (Table 2). None of the four relatively primitive Type A xenoliths contain low-Ca pyroxene. As this mineral is a significant component of the available material we have from HZ (Nwe, 1976) it suggests a source other than HZ. The generally low values of Θ_{cpp} in these xenoliths are consistent with a source in HZ (Fig. 12) although this is not diagnostic, telling us only that cooling was relatively rapid.

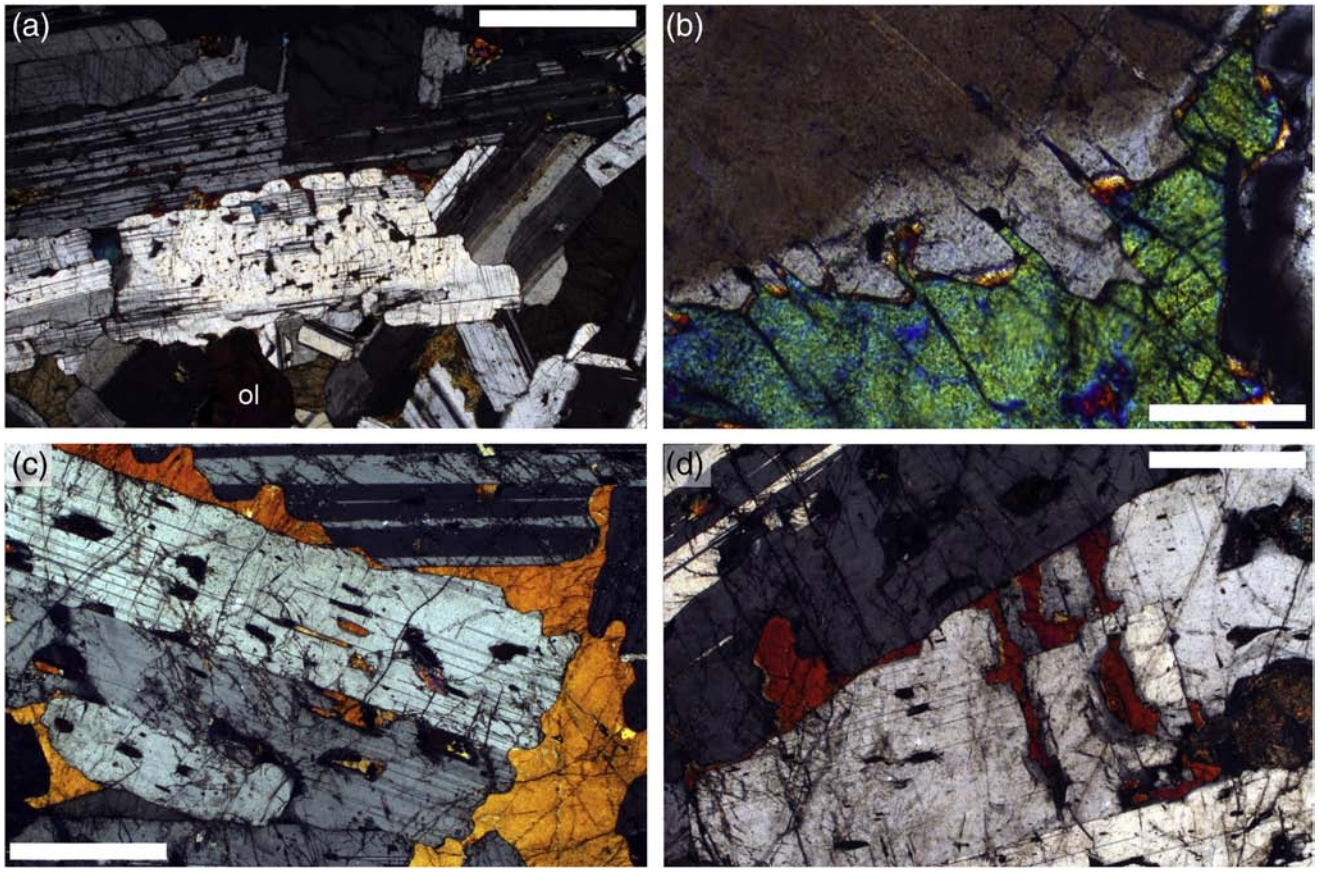

Fig. 10. Type B xenoliths from the Campsite Dyke. (a) Sample SKG11-11-4. Large plagioclase primocrysts with irregular margins are rich in melt inclusions, whereas smaller plagioclase grains are free of melt-inclusions. Note the rounded olivine primocryst (ol) and the highly irregular and cuspate grains of interstitial augite. Crossed polars. Scale bar is 1 mm long. (b) Sample SKG11-11-5. Intimate and irregular intergrowth of interstitial augite and the edge of the plagioclase primocryst. Note how the plagioclase of the intergrowth has a different birefringence (it is more albitic) than the older part of the grain. Crossed polars. Scale bar is 200 μm long. (c) Sample SKG11-11-5. Irregular morphology of interstitial augite reflecting the irregular shape and rounded, anhedral, ends of the plagioclase primocrysts. Note how the interstitial augite is in optical continuity with augite within pockets in the plagioclase grain. Several of these augite pockets also contain finely crystallised material identical to that in the melt inclusions — these augite grains therefore grew into original melt-filled pockets in the plagioclase. Crossed polars. Scale bar is 1 mm long. (d) Sample SKG11-11-5. Note the irregular morphology of interstitial augite at the grain boundary between two plagioclase primocrysts. The augite grows into the lower of the two plagioclases, with more sodic plagioclase adjacent to the ingrowths. Crossed polars. Scale bar is 1 mm long.

Microstructures of the Type A xenoliths are consistent with formation in a simple magma chamber, with a generally monotonic cooling rate and active fractionation (since highly evolved interstitial material is not abundant). Partial melting occurred only in the vicinity of evolved interstitial phases and in the thick, relatively sodic rims of the plagioclase grains. We conclude that it is entirely possible that the source of these xenoliths (with the exception of SKG11-11-1) is some deep, hitherto unknown, region of the Skaergaard chamber, or some other similar chamber in which the magma was saturated only in plagioclase and olivine (± augite). The cooling rate of this chamber is likely to have been similar to that of the Skaergaard chamber, given the similarity of grain size and Θ_{cpp} to the lowermost parts of the Skaergaard stratigraphy.

Type B xenoliths have distinctive microstructures that are very different to those developed in layered intrusions. It is instructive to compare their microstructures with those of the Icelandic nodules, with which they have much in common.

The marked marginal zoning of the primocryst phases (particularly plagioclase, Fig. 11d, f), and the contrast between the large primocrysts and the fine-grained intergrowths in the melt pools (Fig. 11a), in the Icelandic nodules points to a multi-stage solidification history. Initial slow cooling produced a population of large, equant crystals. The multitude of melt inclusions in the plagioclase grains was most probably created during this first growth stage — these inclusions have sodic walls (Fig. 11d) and are therefore unlikely to have formed by melting, as in this case they would have calcic walls (Johannes et al., 1994). At the end of the first stage of solidification the nodules comprised a crystal framework with abundant interstitial liquid. The plagioclase grains had rounded and irregular margins, with abundant thick melt films between them (Fig. 11b). Very few three-grain junctions were formed at this stage (c.f. Holness et al., 2012a,b). The second stage of solidification involved a much faster crystallisation rate, with the formation of cellular features on previously smooth growth faces, dendritic and hopper-like extensions on primocrysts, the formation of fine-grained intergrowths of augite and plagioclase (Fig. 11a), and the growth of augite into melt inclusions and melt films on grain boundaries (Fig. 11c, e). Three-grain junctions were formed during this phase, with a low median angle (though this wasn't measured for the Icelandic nodules, the planar augite–plagioclase boundaries demonstrate the median would be close to 78° were sufficient junctions present to permit the collection of meaningful data). That these nodules are found in glassy and very fine-grained extrusive rocks (Hansen and Grönvold, 2000) demonstrates that the second solidification stage observed in the nodules occurred before eruption at the surface. A plausible interpretation of the microstructures we see is that the nodules were broken off and removed from a deep, slowly-cooling source and were then moved into a smaller body of magma, most likely a conduit, where they remained for sufficient time to create the secondary solidification features during rapid cooling. They were then entrained and erupted, with quenching of the microstructures.

The Type B xenoliths have the same inclusion-rich plagioclase, with rounded irregular shapes and sharply-defined sodic rims, as the

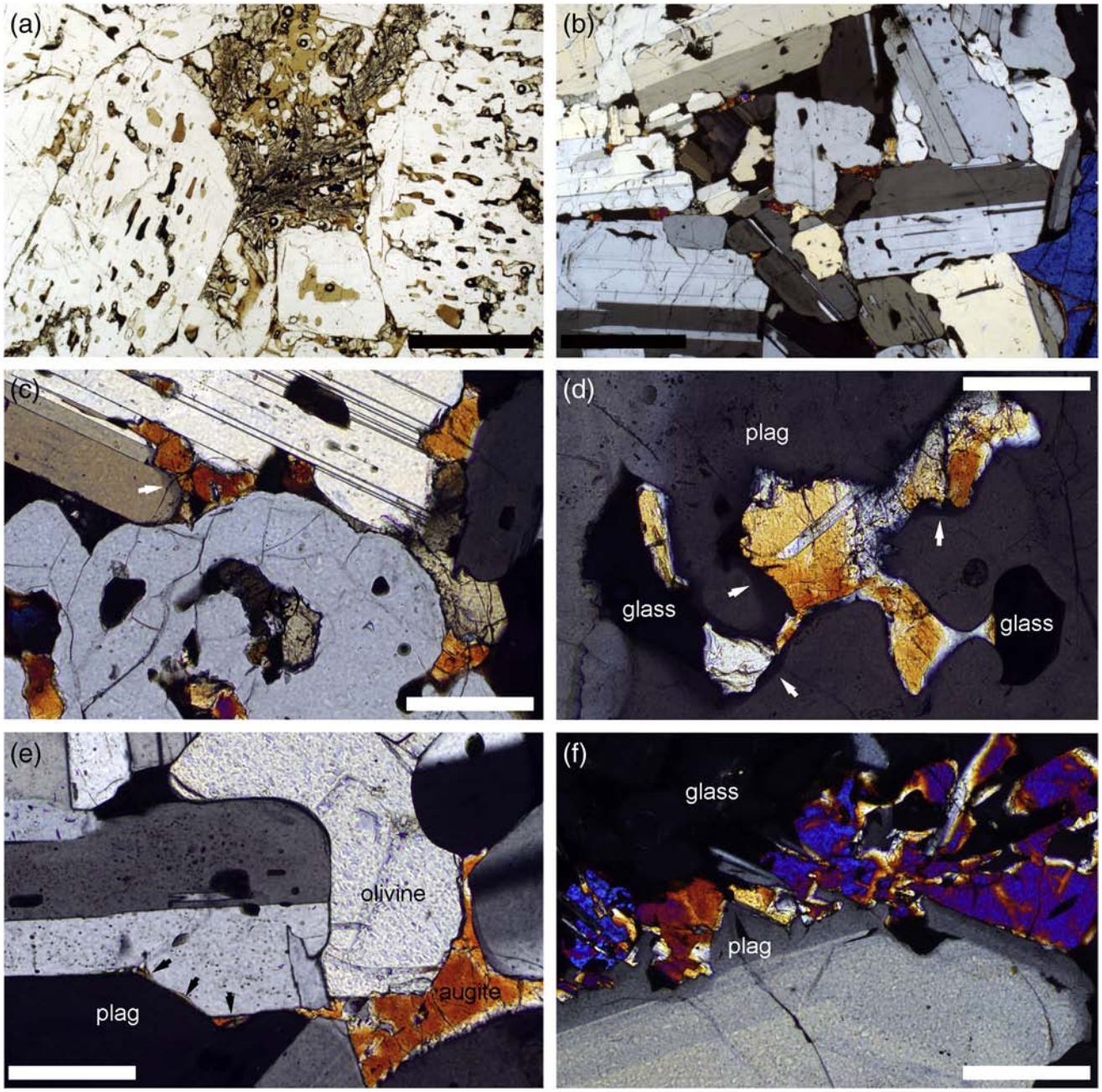

Fig. 11. Photomicrographs of the Icelandic glassy crystalline nodules. (a) FON02B. This sample comprises large, rounded, plagioclase crystals with abundant glassy melt inclusions. The interstitial spaces between the plagioclase grains are filled with brown glass and turbid intergrowths of plagioclase, augite and olivine. Plane polarized light. Scale bar is 1 mm long. (b) FON02B. Note the irregular, rounded margins of the plagioclase grains and their random orientation. The irregular, sometimes cuspate, melt-filled spaces between them are variably filled with augite which necessarily takes on an irregular morphology. Crossed polars. Scale bar is 1 mm long. (c) FON02B. Augite partially fills thick, irregular melt-filled pockets between large plagioclase grains and fills some melt inclusions. Note the sodic rims to the infilled melt inclusions. Cross polars. Scale bar is 200 μm long. (d) FON02B. Highly irregular melt inclusion that is partially filled with augite. Note the discontinuous and irregular sodic rims to the inclusion (arrowed). Crossed polars. Scale bar is 100 μm long. (e) SAX02. Augite fills the spaces between large primocrysts of olivine and plagioclase. Whereas the olivine grain has not grown into the melt-filled space at the top of the image, augite has filled much smaller spaces, with low dihedral angles at the corners (arrowed). Crossed polars. Scale bar is 200 μm long. (f) FON04A. The margins of the large plagioclase primocrysts are irregular where in contact with large melt pools. The margin of this grain is formed of a symplectite-type intergrowth of augite and plagioclase. Note the sodic rim with the planar internal margin indicative of an early growth stage with planar growth faces, followed by rapid growth in a eutectic-like relationship with the augite. Crossed polars. Scale bar is 200 μm long.

Icelandic nodules. While augite forms large grains, we suggest it is only the cores of these grains that were primocrysts, whereas the marginal parts of the augite grains grew during a second, more rapid, phase of solidification. Supporting evidence is provided by the augite growing in some melt inclusions and the irregular attenuated interstitial grains that have grown into what must have been thick melt films separating plagioclase grains (Fig. 10c, d). Θ_{cpp} is low, attesting to rapid crystallisation during the formation of the three-grain junctions during a secondary crystallisation event. We suggest the intergrowths of sodic plagioclase and augite on grain boundaries (Fig. 10b) are analogous to the finer intergrowths of augite and plagioclase seen in the Icelandic nodules, but their smaller size and larger grain size suggests that the crystallisation rate during the second growth stage was not as rapid as that experienced by the Icelandic nodules.

This kind of multi-stage cooling history is not possible in a large layered intrusion. Instead the Type B xenoliths must have been removed

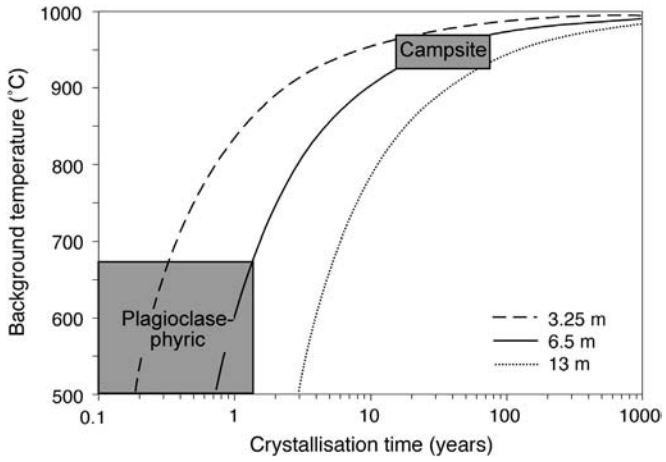

Fig. 12. The variation of crystallisation time in the centre of dykes of thickness, 3.25, 6.5 and 13 m thickness as a function of country rock temperature. The two grey boxes constrain the country rock temperatures using the crystallisation times determined from Θ_{cpp} according to the empirical relationship of Holness et al. (2012b).

as discrete, partially crystallised, blocks from a deep chamber and retained at an intermediate position, perhaps in some kind of conduit, for the second, more rapid, crystallisation event, before being brought to their present position in the Campsite Dyke. It is not likely that the intermediate position was actually their present position because the cooling rate of the Campsite Dyke resulted in relatively high dihedral angles, whereas the lower angles in the Type B xenoliths point to a more rapid rate of solidification during the second stage.

It is highly unlikely that they were derived from the Layered Series of the Skaergaard since the xenoliths were clearly melt-bearing when removed from their source and the lower part of the Skaergaard was undoubtedly entirely solidified when the Campsite Dyke intruded. Instead we propose that the Type B xenoliths were derived from some other deep magma body, and experienced a multi-stage entrainment process, during which they became entirely solidified, before being taken up by the Campsite Dyke magma and brought to their present position.

9.3. Constraints on the thermal history of the Layered Series

The preliminary examination of the pyroxenes in SKG11-11-1 provides a number of constraints on the thermal history of the lower part of the Layered Series.

Pyroxenes in the lower part of the Layered Series are typified by evidence of multi-stage exsolution indicative of an early monoclinic stage for low-Ca pyroxenes (e.g. Nwe, 1976). The presence of inverted pigeonite in the exposed Layered Series, and in the Cambridge drill core, is indicated by the blebby nature of the early generation of Ca-rich exsolution lamellae (which exsolved close to the (001) planes of the original monoclinic structure) in contrast to the more regular and planar nature of the later exsolution which formed lamellae close to (100) of the inverted orthorhombic structure. Exsolution of low-Ca pyroxene in the augite is similarly multi-stage although the early stage is not generally as blebby as in the inverted pigeonite. Un-inverted pigeonite is absent in the lower part of the Layered Series, although it may comprise up to 10% of the low-Ca pyroxene in UZ just before primary pigeonite disappears (Brown, 1957).

The only low-Ca pyroxene-bearing xenolith studied here is SKG11-11-1. (Note that although the others might have contained low-Ca pyroxene that has subsequently been altered beyond recognition, the absence of optically visible exsolution lamellae in the augite suggests no low-Ca pyroxene was ever present). This sample contains partially inverted pigeonite, with planar exsolution lamellae. For pigeonite of X_{Fe} of 0.476 the inversion to hypersthene should occur at 1040 ± 10 °C (Ishii, 1975). However, inversion may occur by three separate mechanisms and the kinetics of the inversion are unknown (Buseck et al., 1980). Despite this, we can place approximate constraints on the timing of inversion relative to entrainment of the block by comparison with pigeonite occurrences in igneous bodies of known dimension and cooling rate.

Wholly un-inverted pigeonite is found in the centre of the Whin Sill where it is penetrated by the Throckley borehole (Dunham et al., 1972). Here the sill is ~38 m thick and Θ_{cpp} in the dolerites at the centre of the sill is 87 ± 4° (Holness et al., 2012b). The similarity of the Whin Sill Θ_{cpp} with that in the Campsite Dyke suggests the post-entrainment thermal history of the xenoliths was similar to that of the central part of the Whin. Cooling rates in these two environments were therefore too fast to permit pigeonite inversion. A further comparison can be made with the ~300 m thick Nipissing Sill in which un-inverted pigeonite, together with partially and entirely inverted pigeonite, is found (Hriskevich, 1968). The cooling rate in the centre of the Nipissing Sill is likely to have been similar to that in the centre of the 266 m thick Basement Sill at West Bull Pass, where Θ_{cpp} is 100 ± 2° (Holness et al., 2012b). The cooling rate required to permit pigeonite inversion is therefore significantly lower than was likely to have been experienced post-entrainment in the Campsite Dyke. These observations suggest that the partial inversion of the pigeonite in block SKG11-11-1 may have occurred before entrainment. The low-Ca pyroxenes in LZb (and, by extension, in all Layered Series rocks overlying LZb) were likely

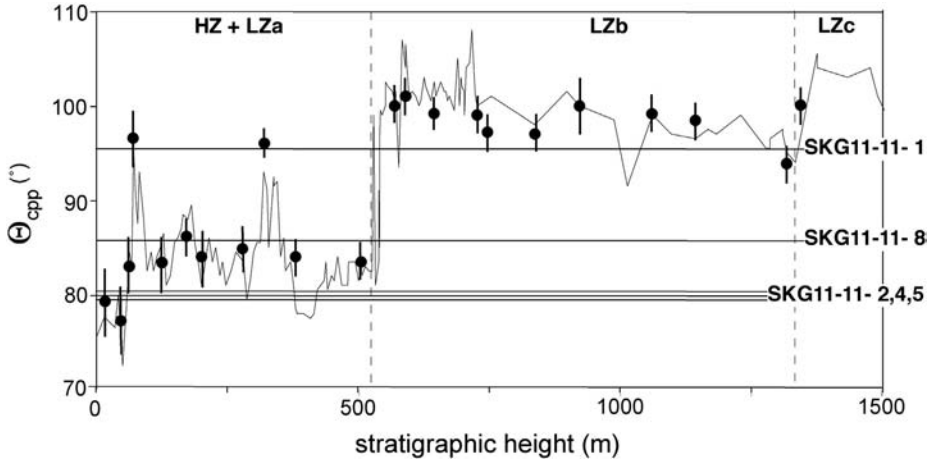

Fig. 13. The variation of Θ_{cpp} with stratigraphy in the Skaergaard Layered Series and HZ, taken from Holness et al. (2007a,c) and Holness et al. (in press). The values of Θ_{cpp} determined from the xenoliths are shown, for comparison.

therefore to have been still mostly monoclinic at the time of injection of the Campsite Dyke.

The width, spacing, crystallographic orientation and composition of exsolution lamellae can be used to deduce cooling rates (e.g. Brearley, 1991; McCallum and O'Brien, 1996), although hydrothermal circulation may influence the thickness of the lamellae (Taylor and Forester, 1979). Thermometry on the wide set of exsolution lamellae in the pigeonite (those in the augite are too narrow for conventional electron microprobe analysis) using the QUILF thermometer results in an average temperature of 820 °C, with a standard deviation of 26 °C — this is close to the likely closure temperature for Ca–Fe–Mg diffusion in pyroxene (McCallum and O'Brien, 1996). The presence of two distinct sets of exsolution lamellae in both the augite and the pigeonite suggest a multi-stage cooling history — it is likely that this reflects an initial slow cooling rate from the liquidus while in situ in LZb, followed by a more rapid cooling following entrainment and emplacement as a block in the Campsite Dyke. It would be instructive to undertake a more detailed study of these two exsolution generations.

10. Conclusions

The cooling rate information preserved by the average grain size and the geometry of three-grain junctions in the Campsite and Plagioclase-phyric dykes points to the Campsite Dyke being the older of the two. Simple thermal models suggest that this early dyke was emplaced in the Skaergaard Intrusion while the surrounding cumulates were just below their likely solidus temperatures. The Plagioclase-phyric Dyke was emplaced later, once the Skaergaard UZ cumulates had cooled below 670 °C.

Only one of a suite of eight gabbroic troctolite xenoliths (sample SKG11-11-1) collected at random from the Campsite Dyke is likely to have been sourced from the Skaergaard itself. The highly melt inclusion-rich xenoliths studied by Jakobsen et al. (2010) display distinctive microstructural and compositional characteristics indicative of a two-stage cooling history prior to entrainment in the Campsite Dyke. We suggest this type of xenolith is formed from blocks derived from some deeper intrusion that had a multi-stage ascent to their present level of exposure. The similarity of compositions of the melt inclusions and plausible Skaergaard parental liquids, as discussed by Jakobsen et al. (2010), is most likely due to the development of many compositionally related intrusions in the deep crust underlying the East Greenland margin.

Acknowledgments

We thank Madeleine Humphreys for her assistance in collecting samples from the Campsite area. We are grateful to Monica Price of the Oxford University Natural History Museum for access to samples from the Wager East Greenland collection, and to Christian Tegner and Kent Brooks for loan of the sample from the Campsite Dyke chill zone. John Maclennan loaned us material from Iceland and we both thank him and David Neave for interesting discussions about their microstructures. Insightful and helpful comments from Tony Morse and an anonymous reviewer greatly improved an earlier version of this contribution. QEMSCAN® is a registered trademark of FEI Company. FEI Company sponsored the QEMSCAN® analyses, which were completed by Dr Gavyn Rollinson, at Camborne School of Mines, University of Exeter, UK. This work was supported by the Natural Environment Research Council [grant numbers NE/F020325/1 and NE/J021520/1].

References

Andersen, D.J., Lindsley, D.H., Davidson, P.M., 1993. QUILF: a Pascal program to assess equilibria among Fe–Mg–Mn–Ti oxides, pyroxenes, olivine, and quartz. Computers and Geosciences 19, 1333–1350.

Brearley, A.J., 1991. Subsolidus microstructures and cooling history of pyroxenes in the zagami shergottite. Abstracts of the Lunar and Planetary Science Conference 22, 135.

Brooks, C.K., Nielsen, T.F.D., 1978. Early stages in the differentiation of the Skaergaard magma as revealed by a closely related suite of dike rocks. Lithos 11, 1–14.

Brown, G.M., 1957. Pyroxenes from the early and middle stages of fractionation of the Skaergaard intrusion, East Greenland. Mineralogical Magazine 238, 511–543.

Buseck, P.R., Nord Jr., G.L., Veblen, D.R., 1980. Subsolidus phenomena in pyroxenes. Reviews in Mineralogy 7, 117–212.

Cashman, K.V., 1993. Relationship between plagioclase crystallisation and cooling rate in basaltic melts. Contributions to Mineralogy and Petrology 113, 126–142.

Dunham, A.C., Copley, P.A., Strasser-King, V.H., 1972. Submicroscopic exsolution lamellae in pyroxenes in the Whin Sill, Northern England. Contributions to Mineralogy and Petrology 37, 211–220.

Ghiorso, M.S., Sack, R.O., 1995. Chemical mass transfer in magmatic processes IV. A revised model and internally consistent thermodynamic model for the interpolation and extrapolation of liquid–solid equilibria in magmatic systems at elevated temperatures and pressures. Contributions to Mineralogy and Petrology 119, 197–212.

Gottlieb, P., Wilkie, G., Sutherland, D., Ho-Tun, E., Suthers, S., Perera, K., Jenkins, B., Spencer, S., Butcher, A., Rayner, J., 2000. Using quantitative electron microscopy for process mineralogy applications. Journal of the Minerals, Metals and Materials Society 52, 24–27.

Grove, T.L., 1982. Use of exsolution lamellae in lunar clinopyroxenes as cooling rate speedometers: an experimental calibration. American Mineralogist 67, 251–268.

Hansen, H., Grönvold, K., 2000. Plagioclase ultraphyric basalts in Iceland: the mush of the rift. Journal of Volcanology and Geothermal Research 9, 32–81.

Higgins, M.D., 1998. Origin of anorthosite by textural coarsening: quantitative measurements of a natural sequence of textural development. Journal of Petrology 39, 1307–1323.

Hjartarson, Á., 1988. Þjórsárhraunið mikla-stærsta nútímahraun jarðar. Natturufraedingurinn 58, 1–16 (in Icelandic).

Holness, M.B., Sawyer, E.W., 2008. On the pseudomorphing of melt-filled pores during the crystallization of migmatites. Journal of Petrology 49, 1343–1363.

Holness, M.B., Anderson, A.T., Martin, V.M., Maclennan, J., Passmore, E., Schwindinger, K., 2007a. Textures in partially solidified crystalline nodules: a window into the pore structure of slowly cooled mafic intrusions. Journal of Petrology 48, 1243–1264.

Holness, M.B., Nielsen, T.F.D., Tegner, C., 2007b. Textural maturity of cumulates: a record of chamber filling, liquidus assemblage, cooling rate and large-scale convection in mafic layered intrusions. Journal of Petrology 48, 141–157.

Holness, M.B., Tegner, C., Nielsen, T.F.D., Stripp, G., Morse, S.A., 2007c. A textural record of solidification and cooling in the Skaergaard Intrusion, East Greenland. Journal of Petrology 48, 2359–2377.

Holness, M.B., Humphreys, M.C.S., Sides, R., Helz, R.T., Tegner, C., 2012a. Towards an understanding of disequilibrium dihedral angles in mafic rocks. Journal of Geophysical Research. http://dx.doi.org/10.1029/2011JB008902.

Holness, M.B., Richardson, C., Helz, R.T., 2012b. Disequilibrium dihedral angles in dolerite sills: a new proxy for cooling rate. Geology 40, 795–798.

Holness, M.B., Namur, O., Cawthorn, R.G., 2013. Disequilibrium dihedral angles in layered intrusions: a microstructural record of fractionation. Journal of Petrology 54, 2067–2093.

Hoover, J.D., 1989. Petrology of the marginal border series of the Skaergaard Intrusion. Journal of Petrology 30, 399–439.

Hriskevich, M.E., 1968. Petrology of the Nipissing Diabase Sill, of the Cobalt Area, Ontario, Canada. Geological Society of America Bulletin 79, 1387–1404.

Irvine, T.N., Andersen, J.C.O., Brooks, C.K., 1998. Included blocks (and blocks within blocks) in the Skaergaard intrusion: geologic relations and the origins of rhythmic modally graded layers. Geological Society of America Bulletin 110, 1398–1447.

Ishii, T., 1975. The relations between temperature and composition of pigeonite in some lavas and their application to geothermometry. Mineralogical Journal of Japan 8, 48–57.

Jakobsen, J.K., Tegner, C., Brooks, C.K., Kent, A.J.R., Lesher, C.E., Nielsen, T.F.D., Widenbeck, W., 2010. Parental magma of the Skaergaard intrusion: constraints from melt inclusions in primitive troctolite blocks and FG-1 dykes. Contributions to Mineralogy and Petrology 159, 61–79.

Johannes, W., Koepke, J., Behrens, H., 1994. Partial melting reactions of plagioclase and plagioclase-bearing systems. In: Parsons, I. (Ed.), Feldspars and their Reactions. Kulwer Academic Publishers, Netherlands, pp. 161–194.

Kudo, A.M., Weill, D.F., 1970. An igneous plagioclase thermometer. Contributions to Mineralogy and Petrology 25, 52–65.

Larsen, R.B., Tegner, C., 2006. Pressure conditions for the solidification of the Skaergaard intrusion: eruption of East Greenland flood basalts in less than 300 000 years. Lithos 92, 181–197.

Lindsley, D.H., Andersen, D.J., 1983. A two-pyroxene thermometer. Journal of Geophysical Research 88, A887–A906.

Maaløe, S., 1976. Zoned plagioclase of the Skaergaard Intrusion, East Greenland. Journal of Petrology 17, 398–419.

McBirney, A.R., Naslund, H.R., 1990. The differentiation of the Skaergaard Intrusion. Contributions to Mineralogy and Petrology 104, 235–240.

McCallum, I.S., O'Brien, H.E., 1996. Stratigraphy of the lunar highland crust: depths of burial of lunar samples from cooling-rate studies. American Mineralogist 81, 1166–1175.

Morse, S.A., 2001. Augite–olivine equilibria in the Kiglapait Intrusion, Labrador, Canada. Canadian Mineralogist 39, 267–274.

Morse, S.A., 2008. Toward a thermal model for the Skaergaard liquids. American Mineralogist 93, 248–251.

Morse, S.A., 2011. The fractional latent heat of crystallizing magmas. American Mineralogist 96, 682–689.

Morse, S.A., Lindsley, D.H., Williams, R.J., 1980. Concerning intensive parameters in the Skaergaard Intrusion. American Journal of Science 280A, 159–170.
Namur, O., Humphreys, M., Holness, M.B., 2013. Thermal buffering during solidification of a gabbroic crystal mush: Skaergaard Intrusion, Greenland. Journal of Petrology (submitted for publication).
Nielsen, T.F.D., 1978. The Tertiary dike swarms of the Kangerdlugssuaq area, East Greenland. An example of magmatic development during continental break-up. Contributions to Mineralogy and Petrology 67, 63–78.
Nielsen, T.F.D., 2004. The shape and volume of the Skaergaard Intrusion. Greenland: implications for mass balance and bulk composition. Journal of Petrology 45, 507–530.
Nwe, Y.Y., 1976. Electron-probe studies of the earlier pyroxenes and olivines from the Skaergaard intrusion, East Greenland. Contributions to Mineralogy and Petrology 55, 105–126.
Pirrie, D., Butcher, A.R., Power, M.R., Gottlieb, P., Miller, G.L., 2004. Rapid quantitative mineral and phase analysis using automated scanning electron microscopy (QEMSCAN®); potential applications in forensic geoscience. Geological Society Special Publication 232, 123–136.
Salmonsen, L.P., Tegner, C., 2013. Crystallisation sequence of the Upper Border Series of the Skaergaard Intrusion: revised subdivision and implications for chamber-scale magma homogeneity. Contributions to Mineralogy and Petrology 165, 1155–1171.
Schiavi, F., Walte, N., Keppler, H., 2009. First in situ observation of crystallization processes in a basaltic–andesitic melt with the moissanite cell. Geology 37, 963–966.
Stickels, C.A., Hücke, E.E., 1964. Measurement of dihedral angles. Transactions of the Metallurgical Society of AIME 230, 795–801.
Taylor Jr., H.P., Forester, R.W., 1979. An oxygen and hydrogen isotope study of the Skaergaard Intrusion and its country rocks: a description of a 55-m.y. old fossil hydrothermal system. Journal of Petrology 20, 355–419.
Thordarson, T., Self, S., Miller, D.J., Larsen, G., Vilmundardóttir, E.G., 2003. Sulphur release from flood lava eruptions in the Veiðivötn, Grimsvötn and Katla volcanic systems, Iceland. In: Oppenheimer, C., Pyle, D.M., Barclay, J. (Eds.), Volcanic Degassing. Geological Society of London, Special Publication, 213.
Thy, P., Tegner, C., Lesher, C.E., 2009. Liquidus temperatures of the Skaergaard magma. American Mineralogist 94, 1371–1376.
Vincent, E.A., 1953. Hornblende-lamprophyre dykes of basaltic parentage from the Skaergaard area, East Greenland. Quarterly Journal of the Geological Society of London 109, 21–51.
Wager, L.R., Deer, W.A., 1939. Geological investigations in East Greenland. Pt III. The petrology of the Skaergaard intrusion. Kangerdlugssuaq, East Greenland. Meddeleser om Grønland 105, 1–352.
Williams, R.J., 1971. Reaction constants in the system Fe–MgO–SiO_2–O_2: intensive parameters in the Skaergaard Intrusion, East Greenland. American Journal of Science 271, 132–146.